The Astrophysical Journal Supplement Series, 239:5 (18pp), 2018 November https://doi.org/10.3847/1538-4365/aae155

A *TESS* Dress Rehearsal: Planetary Candidates and Variables from *K2* Campaign 17

Ian J. M. Crossfield[1], Natalia Guerrero[1], Trevor David[2], Samuel N. Quinn[3], Adina D. Feinstein[4], Chelsea Huang[1], Liang Yu[1], Karen A. Collins[3], Benjamin J. Fulton[5], Björn Benneke[6], Merrin Peterson[6], Allyson Bieryla[3], Joshua E. Schlieder[7], Molly R. Kosiarek[8,16], Makennah Bristow[9], Elisabeth Newton[1,17], Megan Bedell[10], David W. Latham[3], Jessie L. Christiansen[5], Gilbert A. Esquerdo[3], Perry Berlind[3], Michael L. Calkins[3], Avi Shporer[1], Jennifer Burt[1], Sarah Ballard[1], Joseph E. Rodriguez[3], Nicholas Mehrle[1], Courtney D. Dressing[11], John H. Livingston[12], Erik A. Petigura[8,18], Sara Seager[1,13], Jason Dittmann[1], David Berardo[1], Lizhou Sha[1], Zahra Essack[13], Zhuchang Zhan[13], Martin Owens[1], Isabel Kain[1], Howard Isaacson[11], David R. Ciardi[5], Erica J. Gonzales[14,16], Andrew W. Howard[8], and José Vinícius de Miranda Cardoso[15]

[1] Department of Physics, and Kavli Institute for Astrophysics and Space Research, Massachusetts Institute of Technology, Cambridge, MA 02139, USA
[2] Jet Propulsion Laboratory, California Institute of Technology, 4800 Oak Grove Drive, Pasadena, CA 91109, USA
[3] Center for Astrophysics, 60 Garden Street, Cambridge, MA 02138, USA
[4] Department of Physics and Astronomy, Tufts University, Medford, MA 02155, USA
[5] Caltech/IPAC-NASA Exoplanet Science Institute, 770 S. Wilson Avenue, Pasadena, CA 91106, USA
[6] Departement de Physique, Universite de Montreal, Montreal, H3T 1J4, Canada
[7] NASA Goddard Space Flight Center, 8800 Greenbelt Road, Greenbelt, MD 20771, USA
[8] Cahill Center for Astrophysics, California Institute of Technology, Pasadena, CA 91125, USA
[9] Department of Physics, University of North Carolina at Asheville, Asheville, NC 28804, USA
[10] Center for Computational Astrophysics, Flatiron Institute, 162 5th Avenue, New York, NY 10010, USA
[11] Astronomy Department, University of California, Berkeley, CA, USA
[12] Department of Astronomy, Graduate School of Science, The University of Tokyo, Hongo 7-3-1, Bunkyo-ku, Tokyo, 113-0033, Japan
[13] Department of Earth, Atmospheric and Planetary Sciences, Massachusetts Institute of Technology, Cambridge, MA 02139, USA
[14] Department of Astronomy and Astrophysics, University of California, Santa Cruz, CA 95064, USA
[15] Universidade Federal de Campina Grande, Campina Grande, Brazil

Received 2018 June 8; revised 2018 September 4; accepted 2018 September 11; published 2018 November 5

Abstract

We produce light curves for all ∼34,000 targets observed with *K2* in Campaign 17 (C17), identifying 34 planet candidates, 184 eclipsing binaries, and 222 other periodic variables. The forward-facing direction of the C17 field means follow-up can begin immediately now that the campaign has concluded and interesting targets have been identified. The C17 field has a large overlap with C6, so this latest campaign also offers an infrequent opportunity to study a large number of targets already observed in a previous *K2* campaign. The timing of the C17 data release, shortly before science operations begin with the *Transiting Exoplanet Survey Satellite* (*TESS*), also lets us exercise some of the tools and methods developed for identification and dissemination of planet candidates from *TESS*. We find excellent agreement between these results and those identified using only *K2*-based tools. Among our planet candidates are several planet candidates with sizes $<4\,R_\oplus$ and orbiting stars with $Kp \lesssim 10$ (indicating good RV targets of the sort *TESS* hopes to find) and a Jupiter-sized single-transit event around a star already hosting a 6 day planet candidate.

Key words: methods: data analysis – planets and satellites: detection – techniques: photometric

Supporting material: machine-readable tables

1. Introduction

Launched in 2009, the success of *Kepler* and its extended mission, *K2*, is unprecedented. In addition to their considerable contributions to other areas of astrophysics, these missions have led to planet candidates and confirmed planets in the thousands (*Kepler*) and hundreds (*K2*). Unlike the original *Kepler* mission, *K2* observes along the ecliptic plane, providing 30 minute cadence light curves for several thousand targets in each roughly 80 day campaign (Howell et al. 2014).

The surge of data provided by the mission at the end of each campaign is processed and vetted for potential planet candidates. Due to spacecraft systematics and various sources of astrophysical variability, systems showing interesting signals are vetted by-eye before proceeding with additional confirmation follow-up with ground-based telescopes (Montet et al. 2015; Crossfield et al. 2016; Vanderburg et al. 2016; Mayo et al. 2018; Petigura et al. 2018; Yu et al. 2018).

The recently launched *Transiting Exoplanet Survey Satellite* (*TESS*) will observe ∼90% of the sky, approximately 400 times what *Kepler* observed and 26 times what *K2* has observed so far. While experience shows that the vetting of potential planet candidates from *K2* campaigns can be completed by a single person or a small team, the number of *TESS* candidates to be sifted may be far larger. Partly for that reason, *TESS* employs a larger and better-funded team that has been preparing a set of advanced diagnostics and tools. Because *TESS* observes in the anti-Sun direction while orbiting the Earth (Ricker et al. 2014),

[16] NSF Graduate Research Fellow.
[17] NSF Postdoctoral Fellow.
[18] NASA Hubble Fellow.

if *TESS* candidates can be quickly identified after each sector, they can be immediately sent to ground-based observers to confirm the planets and study them in more detail.

The recent delivery of data from *K2* Campaigns 16 and 17 (C16 and C17) have provided us with the chance to exercise some of the tools and techniques being developed for rapid planet candidate identification and dissemination from *TESS* and compare results to previous techniques used for *K2*. We conducted a rapid analysis of data from C16 using tools and methods developed strictly for *K2* (Yu et al. 2018). With C17, we include a more *TESS*-like analysis using several of the tools and team members that will soon examine real *TESS* data.

C16 and C17 are also "*TESS*-like" in at least two other ways. First, these are both "forward-facing" campaigns in which the Earth-trailing *K2* observed roughly anti-Sun from the Earth; as will soon be the case for *TESS* sectors, candidates from *K2*'s forward-facing fields can be immediately observed from the ground if identified with sufficient rapidity. Second, both of these fields partially overlap with previous *K2* campaigns: C16 with C5 (observed 2015 April–July) and C17 with C6 (2015 July–September). The rare overlap between C17 and C6 offers an opportunity to study for again a large number of targets previously observed by *K2*. Campaign 18, currently being observed, will also partly overlap C5 and C16. Similarly, repeated observations of the same targets will occur regularly when *TESS* begins near-continuous, year-long observations of the ecliptic poles.

Here, we present the techniques and results of our rapid identification of planet candidates and other astrophysical variables observed in C17. Section 2 details the identification process of planet candidates using methods and tools developed for both *K2* and for *TESS*. Stellar and planet candidate parameters are discussed in Section 3. Section 4 discusses the results from the two independent vetting techniques described in Section 2. Similarities and discrepancies between planet candidates identified in C17 and C6 are discussed in Section 5. We remark on several individually interesting systems in Section 6, and finally conclude in Section 7.

2. Identifying Planet Candidates

K2 observed C17 from March 1 until 2018 May 8. At 68 days, the campaign is slightly shorter than most previous *K2* campaigns. We followed exactly the methods of Yu et al. (2018) to compute photometry and identify transit-like threshold-crossing events (TCEs). As soon as the raw cadence files were transferred from the spacecraft and uploaded to MAST, we downloaded these data and began our analysis. We converted raw *K2* cadence data to target pixel files with `kadenza`[19] (Barentsen & Cardoso 2018), converted pixel files to time-series photometry with `k2phot`[20], and identified TCEs in light curves using `TERRA`[21] (Petigura 2015; Petigura et al. 2018). We have uploaded light curves for all C17 sources outside the solar system in machine-readable format to the ExoFOP-*K2* website.[22]

We identified 1274 TCEs with multi-event statistics (effectively a measure of signal-to-noise) $\geqslant$10, and pursued two parallel paths to winnow down these 1274 TCEs to a list of reliable planet candidates. In one, we used a set of new tools being developed for efficient and robust vetting of candidates expected to be delivered soon by *TESS*; we hereafter refer to this as *TESS*-like candidate vetting. We also employed a so-called *K2*-like vetting approach using a set of *K2*-specific tools and practices that have been refined through the past four years of *K2* operations (Crossfield et al. 2015, 2016, 2017; Obermeier et al. 2016; Schlieder et al. 2016; Sinukoff et al. 2016; Ciardi et al. 2018; David et al. 2018; Petigura et al. 2018; Yu et al. 2018). We outline both approaches below, and later compare the results of each in Section 4.1.

2.1. *TESS-like Vetting*

In this effort we use the `TERRA` data products with the *TESS* Exoplanet Vetter (TEV), which is the web interface tool developed as part of the *TESS* Science Office data pipeline. TEV will be used to identify *TESS* Objects of Interest (TOIs) in the TCEs found in the *TESS* pipeline of record run by the Science Payload Operations Center (SPOC) at NASA/Ames and the internal Quick-Look Pipeline (QLP; C. Huang et al. 2018, in preparation) run at MIT. TEV was developed at MIT by the *TESS* Science Office staff, and will be described in more detail by N. Guerrero et al. (2018, in preparation).

Generally speaking, TEV imports a data delivery into a database and displays various vetting plots and data for the candidate TCEs for the first round of vetting by individuals. The data reduction pipeline that generated the analysis products—in this case `TERRA` (Petigura et al. 2018), but SPOC or QLP for *TESS* science operations—provides an analysis summary page for each candidate TCE and a more comprehensive multi-page analysis report. The pipeline also provides a spreadsheet with the EPIC or TIC ID, and basic stellar and transit parameters.

During the individual vetting phase, human vetters inspect the light curve and other metrics in the analysis summary page (and extended report if necessary) to determine whether the candidate is a planet candidate (PC), eclipsing binary (EB), stellar variability (V), other astrophysical source of variability (O), instrument or systematic noise (IS), or undecided (U). For multi-planet systems, the candidates can be compared consecutively. Each individual vetter assigns a disposition to the candidate and has the option to make additional comments about the candidate. To complete the individual vetting stage, a candidate must get at least three unanimous individual dispositions or up to five total dispositions. The *K2* C17 delivery had 1274 TCEs, roughly half that expected from a typical *TESS* sector. A group of 19 vetters completed the initial vetting stage in less than 24 hours after the delivery was imported into TEV. The final dispositions include 34 planet candidates, 184 eclipsing binaries, and 222 other astrophysical variables, with the rest of the TCEs being instrumental noise or systematics.

TCEs classified unanimously as EB, V, or IS are automatically assigned that value as their final disposition. Targets classified unanimously as PC or with differing dispositions between vetters are flagged for group vetting, the second stage of the vetting process. Once the initial individual vetting concludes, group vetting begins by resolving conflicts for systems classified with at least one planet candidate or undecided disposition. Following this, the group inspects TCEs dispositioned unanimously as planet candidates. Conflicts

[19] https://github.com/KeplerGO/kadenza
[20] https://github.com/petigura/k2phot/
[21] https://github.com/petigura/terra
[22] https://exofop.ipac.caltech.edu/k2/

between EB, V, and IS are resolved last. In this C17 exercise, the group applied and practiced the conventions for assigning candidate dispositions that will be carried over to nominal *TESS* operations, including how to disposition and annotate contact binaries, candidates in a multi-transit system triggered by an eclipsing binary's secondary eclipses, and candidates with radii $>30\,R_\oplus$.

The group vetting process took about three hours to disposition 180 TCEs. This duration is not fixed, and is likely to evolve as *TESS* vetters are trained. Systems identified in the exercise as known planets or eclipsing binaries were still dispositioned as PC, but in nominal *TESS* operations, TEV will filter candidates using catalogs of known planets, eclipsing binaries, and variable stars. Because our analysis uses raw cadence data, we do not expect to recover all C6 candidates identified in previous surveys that used calibrated data products. Nevertheless, several of the candidates identified as strong candidates for observation were known targets in *K2*'s Campaign 6, which demonstrates that TEV users have the materials and expertise necessary to reliably identify planet candidates.

At the conclusion of group vetting, a TEV administrator closed the *K2* C17 delivery to additional changes and TEV generated the final disposition list for download by TEV users. As in nominal *TESS* operations, the final list of C17 planet candidates was disseminated to the *TESS* Follow-Up Observing Program (TFOP[23]).

Although we have endeavored to implement the full *TESS* vetting process, our *K2* C17 vetting diagnostic products did not provide the full diagnostic capabilities that will be available from the SPOC and QLP pipelines for *TESS* vetting. First, no centroid shift information was available to aid in identifying nearby eclipsing binaries from the *K2* data alone, on account of *K2*'s extremely high pointing jitter. Second, the *K2* vetting diagnostics provided access to a light curve from only one photometric aperture per target. *TESS* pipelines will provide light curves from several aperture sizes to help to identify blended EB false positives. Third, the *TESS* analysis will implement ephemeris matching between the 2 minute cadence postage stamps (a restricted set of targets) and the 30 minute cadence full frame images (FFIs) to provide an additional means of identifying *TESS* aperture contamination by near or distant variable sources; we did not employ ephemeris matching in our C17 vetting. Finally, an extensive catalog of known variables and transit false positives is under development. *TESS* TCEs will be automatically crossed-referenced to data in the catalog before the human vetting process begins, but since this catalog is not yet complete we did not cross-reference our C17 candidates against it.

2.2. K2-like Vetting

Our *K2*-like vetting procedure closely followed previous efforts by our group (e.g., Yu et al. 2018). Six participants inspected a subset of TCEs that were assigned in order of TCE number (the EPIC ID appended by the candidate number). This pseudo-random scheme ensured that a given vetter inspected a sample of signals that covered a range of S/N. Each TCE was inspected by at least one person, and by the end of the vetting procedure 986 TCEs were inspected by 2 or more people (with 288 inspected by only one person). This resulted in 2548 individual dispositions for the 1274 TCEs, across 87 unique potential candidates.

Of these 87 signals, 45 were consistently identified as planet candidates by at least 2 people and 50 were identified as a candidate by at least one person without contest. While this vetting procedure was necessarily subjective, the common characteristics we looked for in the TERRA diagnostic plots in order to assign the disposition of a candidate were consistent depth, no obvious odd/even variations in depth or transit time that might suggest an EB, lack of an obvious secondary eclipse, and lack of significant phase-coherent out-of-transit variability. We did not penalize signals for being V-shaped alone. However, if a TCE was deep, V-shaped, and long in duration yet still lacked an obvious secondary eclipse, it was ultimately considered a planet candidate but flagged as a possible false positive. Finally, one vetter inspected each of the 87 flagged candidates and issued a final disposition.

The number of candidates that survived this final vetting stage was 53. The candidates that were demoted included one that was a duplicate of an accepted candidate, 19 that were deemed to be spurious (i.e., systematic artifacts) or otherwise failing to have a consistent shape and depth well above the photon noise, 2 that showed out-of-transit variability in phase with the signal in question (EPIC 212641218 and 212869892), and 12 that showed clear signs of being an EB, a duplicate of an EB signal (i.e., half or double the period), or having an ephemeris match to an EB. Finally, the candidates from the *K2*-like vetting were subjected to further cuts, which are described in Section 4.1.

The main difference between the two candidate lists is that the initial *K2*-like list was somewhat more permissive than the *TESS*-like list. Nonetheless, experience shows that both lists will likely contain false positives (especially for the largest candidates; Santerne et al. 2016). Close inspection of the light curves of the final list of planet candidates revealed interesting information about a select number of candidates, which we summarize below in Section 6.

3. Stellar and Planetary Candidate Parameters

At the conclusion of the vetting exercises described above, we have two lists of possible planet candidates with only a few physical parameters known. Of these, the most salient are a candidate's orbital period (shown in Figure 1), along with transit depth and apparent stellar brightness (discussed below). Stellar parameters for C17 stars are not available in the Ecliptic Planet Input Catalog (EPIC) as they were in past *K2* campaigns (Huber et al. 2016), so the next step is to infer physical parameters such as radii and temperatures.

3.1. Ground-based Spectroscopy

Happily, EPIC parameters and ground-based stellar spectroscopy exist for some C17 stars also observed in C6. Dressing et al. (2017a) described medium-resolution infrared spectroscopy of late-type systems using IRTF/SpeX, and Petigura et al. (2018) described high-resolution optical spectroscopy with Keck/HIRES of a broader sample. Numerous spectra have also been acquired with the Tillinghast Reflector Echelle Spectrograph (TRES; Fűrész 2008) and uploaded to the ExoFOP-*K2* website; we describe these observations below. Table 1 lists the key stellar parameters reported for 24 targets in C17 from SpeX, HIRES, and TRES.

[23] https://tess.mit.edu/followup/

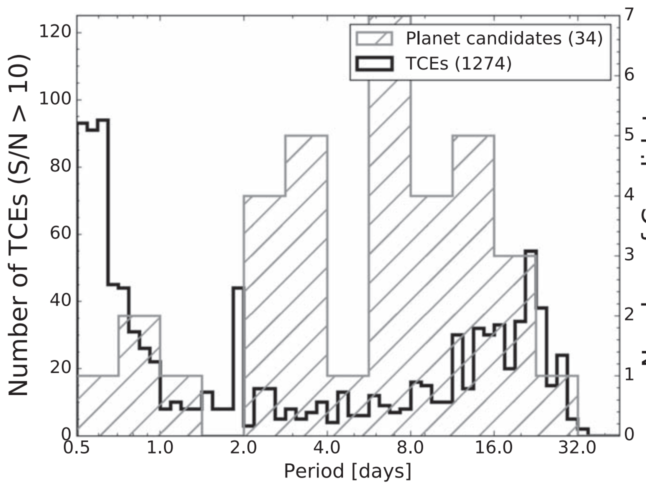

Figure 1. Orbital periods of planet candidates identified in our analysis. The dark, narrow-binned histogram (axis at left) shows the threshold-crossing events (TCEs) identified by TERRA with $S/N \geqslant 10$ (see Section 2). The gray, hatched histogram (axis at right) indicates the distribution of 34 planet candidates.

We also include the parameters of two newly identified candidates orbiting bright stars from C17, EPIC 212628254 and 212779563.

TRES is located on the 1.5 m Tillinghast Reflector at Fred Lawrence Whipple Observatory on Mount Hopkins. TRES is a fiber-fed cross-dispersed echelle spectrograph with a resolving power of $R \approx 44,000$ and an instrumental velocity precision of 10–15 m s^{-1}, well-suited to stellar classification and identification of binaries via radial velocity variations and/or composite spectra. We use the Stellar Parameter Classification (SPC) package (see Buchhave et al. 2012) to determine the effective temperature, surface gravity, metallicity, and rotational broadening of each spectrum, and we report those values in Table 1. We also report the radial velocities derived from the cross-correlation of a single spectral order against the best-matched synthetic spectrum, shifted to the absolute IAU scale. The TRES spectra—along with plots of stellar classifications resulting from cross-correlation against a coarse grid of synthetic spectra and spectral regions of interest—are available on ExoFOP-*K2*.[24]

3.2. Multicolor Photometry and Gaia DR2

Despite the spectroscopic data from SpeX, HIRES, and TRES, we desire a complete and homogeneous set of stellar parameters against which to compare our C17 candidate sample. To this end, we set aside spectroscopic parameters and instead use EPIC multicolor (*BV ugrizJHK*) photometry, parallaxes from *Gaia* DR2 (Gaia Collaboration et al. 2016, 2018), and isochrones[25] (Morton 2015) to derive stellar parameters using the MIST isochrones (Choi et al. 2016; Dotter 2016).

For C6 targets we use the *Gaia–K2* cross-match from https://gaia-kepler.fun. For targets not in C6 we run our own cross-match between the EPIC locations and *Gaia* DR2 using an initial search radius of 5″, selecting the *Gaia* source that most closely matches the position and magnitude of the *K2* target. There were no ambiguous cases. All stars with $|Kp - G| > 0.5$ turned out to be stars where Kp was estimated from 2MASS colors alone. For all planet candidates, we are pleased to find that the distances inferred from isochrones are consistent with those from *Gaia* (at the 3σ level). The inferred stellar parameters for our candidates are listed in Table 2 and are online at ExoFOP-*K2*, and a color–magnitude diagram of our final candidate sample is shown in Figure 2. Our derived stellar radii agree with those from *Gaia* DR2 with a scatter of 5%–10%, suggesting that both sets of radii are consistent at that level.

After inferring stellar parameters for our sample, we then run a final round of light-curve fitting. We follow the same approach used in Crossfield et al. (2016): placing a prior on the quadratic limb-darkening parameters inferred from the assumed stellar parameters using LDTk (Parviainen & Aigrain 2015), then fitting the light curves using BATMAN (Kreidberg 2015).

4. Results and Discussion

4.1. Purifying the Sample

Some of the TCEs that we identified as planet candidates subsequently turned out to be non-planetary. Eleven candidates were identified as planet candidates during *TESS*-like group vetting, but were subsequently eliminated because the implied candidate radii would be $>30\,R_\oplus$. These stars are EPIC 212579164, 212580081, 212627712, 212628098, 212770429, 212651213, 212757601, 212769367, 212769682, 212871068, and 212884586.

For the last of these, 212884586, *Gaia* DR2 shows two stars near the source's location with $G = 19.8$ and 19.6 mag, both located at distances >400 pc and both within the *K2* aperture. Either could be the transit host and the transit would be diluted by the light of the other, in which case our inferred radius of $20^{+21}_{-13} R_\oplus$ would reach $\sim 30\,R_\oplus$. We therefore exclude this system from our planet candidate list.

We list EPIC 212658818 as an EB because its transit depth varies throughout the campaign, both in C17 and in C6. This variation is likely due to the putative transits occurring around a star 12″ to the south that is partly in the *K2* aperture. Ground-based follow-up photometry[26] indicates that this star, fainter by 4.1 mag, is the true host of the eclipses (which have a depth of 42%).

We originally identified an EB and a planet candidate around EPIC 212651213 and 251810686, but then discovered that both EPIC stars target the same system (with an offset in the *K2* data "postage stamp" for EPIC 251810686). We also acquired a light curve[27] confirming an event depth of 9% at our measured ephemeris. However, we remove both systems from our candidate list because this is a known quintuple system with two eclipsing binaries (Rappaport et al. 2016).

We note that several remaining candidates have radii formally below our $30\,R_\oplus$ limit, but are still grazing transits and thus have large radius uncertainties (e.g., 212628477 and 212686312). As currently formulated, the *TESS* vetting process would report these as candidates, so we retain them in our C17 sample with a note in Table 2.

[24] https://exofop.ipac.caltech.edu/k2/
[25] https://github.com/timothydmorton/isochrones/
[26] https://exofop.ipac.caltech.edu/k2/edit_target.php?id=212658818
[27] https://exofop.ipac.caltech.edu/k2/edit_target.php?id=212651213

Table 1
Stellar Parameters

EPIC	Kp (mag)	TRES BJD$_{UTC}$[c] (days)	S/N[d]	T_{eff} (K)	log g (dex)	[M/H] (dex)	$v \sin i$[e] (km s^{-1})	RV[f] (km s^{-1})	HIRES[a] T_{eff} (K)	log g (dex)	[Fe/H] (dex)	$v \sin i$ (km s^{-1})	SpeX[b] SpT	T_{eff} (K)	log g (dex)
212428509	12.5	…	…	…	…	…	…	…	5697	4.25	−0.42	1.7	…	…	…
212435047	12.4	…	…	…	…	…	…	…	5750	4.29	0.01	2.0	…	…	…
212460519	12.4	…	…	…	…	…	…	…	4226[g]	…	−0.17	…	…	…	…
212496592	13.0	2457435.973127	25.4	5177	4.57	0.31	2.8	−9.060	…	…	…	…	…	…	…
212521166	11.6	2457436.932008	27.7	4912	4.57	−0.29	1.7	−21.573	4895	4.64	−0.24	1.9	K2V	4841	4.63
212554013	14.7	…	…	…	…	…	…	…	…	…	…	…	K3V	4388	4.64
212572439	12.8	2457442.944484	16.4	5123	4.57	0.45	6.3	13.835	…	…	…	…	K2V	4972	4.59
212580872	13.0	2457493.742254	30.5	5612	4.45	0.20	3.5	−16.946	…	…	…	…	…	…	…
212586030	11.7	…	…	…	…	…	…	…	4865	3.37	0.38	3.5	…	…	…
212587672	12.2	…	…	…	…	…	…	…	5948	4.49	−0.21	2.1	…	…	…
212619190	12.8	2458273.731631	28.7	5648	4.33	0.04	4.6	29.555	…	…	…	…	…	…	…
212628254	9.7	2458261.733258	51.6	5833	4.40	−0.01	3.0	−28.074	5827[h]	4.31[h]	0.04[h]	…	…	…	…
212628477[i]	12.5	2458274.706803	27.5	…	…	…	…	…	…	…	…	…	…	…	…
212634172	14.8	…	…	…	…	…	…	…	…	…	…	…	M3V	3412	4.86
212651213[i]	10.8	2457439.912117	52.2	…	…	…	…	…	…	…	…	…	…	…	…
”	”	2457448.969440	41.0	…	…	…	…	…	…	…	…	…	…	…	…
”	”	2457449.945082	38.5	…	…	…	…	…	…	…	…	…	…	…	…
”	”	2457450.917452	37.7	…	…	…	…	…	…	…	…	…	…	…	…
”	”	2457451.909447	37.3	…	…	…	…	…	…	…	…	…	…	…	…
”	”	2457452.902042	25.8	…	…	…	…	…	…	…	…	…	…	…	…
”	”	2457454.892102	36.6	…	…	…	…	…	…	…	…	…	…	…	…
”	”	2457470.863085	37.6	…	…	…	…	…	…	…	…	…	…	…	…
212651234[g]	11.1	2457439.929578	49.3	4902	3.50	0.23	2.6	−15.508	…	…	…	…	…	…	…
”	”	2457448.983742	27.1	4853	3.34	0.24	2.9	−15.376	…	…	…	…	…	…	…
”	”	2457452.911059	15.1	4901	3.46	0.39	4.9	−15.350	…	…	…	…	…	…	…
”	”	2457466.925434	32.5	5078	3.94	0.35	2.0	−15.399	…	…	…	…	…	…	…
”	”	2457504.855779	23.4	4807	3.22	0.26	3.9	−15.421	…	…	…	…	…	…	…
”	”	2457511.879130	20.4	4861	3.42	0.30	3.9	−15.631	…	…	…	…	…	…	…
212686205	12.3	2457435.907480	28.2	4635	4.70	−0.23	2.3	−12.053	…	…	…	…	K4V	4470	4.51
212689874	12.3	2457434.882603	29.2	5714	4.55	−0.09	3.0	−14.721	5644	4.36	−0.12	1.7	…	…	…
212697709	12.2	2457439.975173	40.1	5785	4.45	0.31	3.1	−21.995	5719	4.28	0.28	1.6	…	…	…
”	”	2457439.997975	39.6	5733	4.38	0.31	3.6	−22.019	…	…	…	…	…	…	…
”	”	2457475.857401	34.1	5796	4.46	0.32	3.4	−21.918	…	…	…	…	…	…	…
212705192[i]	11.7	2457439.893014	53.7	…	…	…	…	…	…	…	…	…	…	…	…
212735333	12.0	2457439.870513	44.5	5671	4.57	−0.01	2.3	−6.591	5660	4.50	0.09	1.3	…	…	…
212768333	11.0	2457439.037432	54.1	5247	4.61	−0.16	5.2	2.071	…	…	…	…	…	…	…
212779596	11.9	2457437.046415	25.6	4652	4.63	−0.21	2.1	0.092	4507[g]	…	−0.04	…	K5V	4731	4.62
212782836	11.6	…	…	…	…	…	…	…	5418	4.48	−0.42	1.1	…	…	…
212779563	9.8	2458261.725801	45.3	4640	4.68	−0.47	0.8	−46.629	4568[g,h]	…	…	…	…	…	…
212803289	11.0	2457437.035094	42.0	6048	3.79	0.11	11.1	−2.778	6102	3.96	0.20	10.0	…	…	…
”	”	2457447.858765	37.7	5906	3.58	0.03	11.5	−2.559	…	…	…	…	…	…	…
”	”	2457475.842684	29.0	6105	3.87	0.30	12.0	−2.554	…	…	…	…	…	…	…
251539584[i]	10.8	2458274.726575	29.1	…	…	…	…	…	…	…	…	…	…	…	…
”	”	2458276.738180	31.3	…	…	…	…	…	…	…	…	…	…	…	…
251539609[i]	11.0	2458275.698478	35.3	…	…	…	…	…	…	…	…	…	…	…	

Table 1
(Continued)

EPIC	Kp (mag)	TRES: BJD_{UTC}[c] (days)	TRES: S/N[d]	TRES: T_{eff} (K)	TRES: log g (dex)	TRES: [M/H] (dex)	TRES: $v \sin i$[e] (km s^{-1})	TRES: RV[f] (km s^{-1})	HIRES[a]: T_{eff} (K)	HIRES[a]: log g (dex)	HIRES[a]: [Fe/H] (dex)	HIRES[a]: $v \sin i$ (km s^{-1})	SpeX[b]: SpT	SpeX[b]: T_{eff} (K)	SpeX[b]: log g (dex)
"	"	2458276.730773	30.1	⋯	⋯	⋯	⋯	⋯	⋯	⋯	⋯	⋯	⋯	⋯	
251554286	12.1	2458275.686467	30.5	5548	4.44	−0.10	1.0	4.560	⋯	⋯	⋯	⋯	⋯	⋯	⋯

Notes.
[a] HIRES data and analysis described by Petigura et al. (2018).
[b] SpeX data and analysis described by Dressing et al. (2017a).
[c] Date of TRES observation.
[d] Signal-to-noise ratio per resolution element in the wavelength range 5060–5315 Å.
[e] SPC measures the broadening from an edge-on rotator with a fixed macroturbulent velocity of 1 km s^{-1}. Different values of macroturbulence may bias this value for slow rotators. As such, we caution against interpreting this value as $v \sin i$ without further analysis.
[f] The RVs reported here have been shifted onto the IAU scale using standard star velocities, on which, e.g., HD 182488, has an absolute RV of −21.508 (Nidever et al. 2002). The uncertainties of the reconnaissance RVs on the TRES native system are typically on the order of 50 m s^{-1} (also affected by T_{eff}, S/N and $v \sin i$), though the offset to the absolute scale carries similar uncertainty.
[g] Star too cool for SpecMatch analysis (see Petigura et al. 2018).
[h] Star observed with APF instead of HIRES, but stellar parameters inferred using the same approach as described in Petigura et al. (2018).
[i] Multi-lined spectrum.

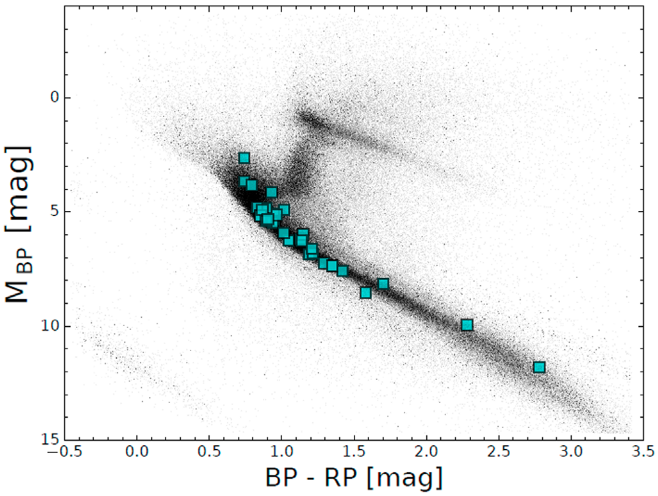

Figure 2. Color–magnitude diagram for our C17 planet candidates (squares) and for all *K2* targets (gray background).

4.2. Planet Candidates, EBs, and Variables

Our *TESS*-like vetting identified 34 planet candidates, all of which were marked as candidates in *K2*-like vetting. Our standard *K2* vetting process identified 53 planet candidates, but several of these were not marked as candidates in *TESS*-like vetting for the following reasons:

1. 251504891.01: marked as variable because of coherent out-of-transit variation.
2. 212473154.01: marked as EB because the candidate radius $R_C = 65\,R_\oplus$.
3. 212789681.01: marked as EB because the transit duration $T_{14} = 0.12$ day is a large fraction of $P = 0.49$ day.
4. 212421319.01: marked as EB because the odd and even transits have different depths.
5. 212499716.01: marked as EB because of a faint secondary eclipse, seen more clearly in C6 photometry.
6. 212579164.01: marked as EB because $R_C = 46\,R_\oplus$.
7. 212580081.01: marked as EB because $R_C = 35\,R_\oplus$.
8. 212627712.01: marked as IS because the *K2* photometric aperture mostly captures light from a nearby, brighter star.
9. 229228115.01: marked as EB because $T_{14} = 0.13$ day is a large fraction of $P = 0.55$ day.
10. 212705192.01: marked as EB because of odd–even effect, and because Keck/HIRES and TRES spectra show the star to be double-lined.
11. 212740148.01: marked as EB because of a faint secondary eclipse. Also, the *K2* photometric aperture mostly captures light from a nearby, brighter star.
12. 212770429.01: marked as IS because the *K2* photometric aperture mostly captures light from a nearby, brighter star.

Table 2 lists the basic parameters for our final list of 34 planet candidates from *K2*'s C17. The properties of this population are also summarized in Figure 1 (orbital periods), Figure 3 (phase-folded candidate light curves), Figure 4 (*Kp* and transit depth), and Figure 5 (candidate radius and insolation).

Though many *K2* planet catalogs have been compared with each other, few have been compared to the CoRoT end-of-mission planet catalog of Deleuil et al. (2018). Figure 1 shows that our C17 candidates have somewhat longer periods than those found by CoRoT (2–16 day versus 1–4 day). *K2* is also sensitive to somewhat smaller planets than CoRoT, as evidenced from the difference between the typical candidate transit depths (0.1% for *K2* C17 versus 0.5% for CoRoT; see Figure 4). There are many differences between the two facilities and their data processing strategies, but the difference in sensitivity of the two missions can be largely attributed to the larger aperture of *Kepler*/*K2* (giving access to shallower transits) and to observing strategy (CoRoT's occasional >80 day campaigns being unable to compensate for its smaller aperture). Simulations of the expected *TESS* yield (Sullivan et al. 2015) similarly show a shallower median transit depth (0.2%), but a longer typical period (2–20 day) due to its year-long coverage of the ecliptic poles.

We also include a list of all likely EBs and other apparently astrophysical variables identified from our *TESS*-like analysis. A total of 184 EBs are listed in Table 3, and 222 variables are listed in Table 4. These tables also include the final comments (if any) assigned to each TCE during the group vetting process. Note also that the numbers above likely somewhat overestimate the objects in each category, since EBs with secondary eclipses and variables with multiple harmonics are both often identified as multiple TCEs in the same system.

5. Comparing Planet Candidates: C17 versus C6

Of our planet candidates (orbiting 18 stars), 24 were also observed by *K2* in C6. This earlier campaign was searched for transiting planets by many groups, giving us a rare opportunity to compare the results of these analyses. Different teams have used a variety of photometric and transit search pipelines, all using fully calibrated data products. Because our analysis here uses raw cadence data (calibrated only by `kadenza`), our noise levels are higher and we do not expect to identify all transit-like signals described in the literature. Although we might naively expect substantial or complete overlap between the C6 surveys, that is not what we find. Table 5 compares the disposition of these 21 C6+C17 candidates by several large-scale surveys, which we describe below.

Pope et al. (2016) identified 19 of our candidates as planet candidates, missing only two of our candidate systems—EPIC 212634172 and 212686205. This is the highest degree of overlap for any C6 catalog, suggesting a higher completeness rate than those of other analyses.

Dressing et al. (2017a, 2017b) derived stellar and planetary parameters and associated false positive probabilities for planets orbiting late-type stars that were discovered by multiple transit surveys. They validated EPIC 212554013 and 212686205, left 212634172 as a planet candidate, and deemed 212572452 to be a false positive because its photometry is blended with that of 212572439.

Mayo et al. (2018) identified and validated planets in 10 of our candidate systems: EPIC 212496592, 212521166, 212580872, 212686205, 212689874, 212697709, 212735333, 212768333, 212779596, and 212803289. They did not report any candidates around our candidate systems EPIC 212554013, 212570977, 212572452, 212572439, 212575828, 212634172, 212661144, or 212813907.

Finally, the signals in 11 of our C6+C17 systems were identified as planet candidates by Petigura et al. (2018), viz., EPIC 212521166, 212554013, 212570977, 212572452,

Table 2
Planet Candidates from C17

Candidate	Kp (mag)	P (day)	T_0 $\mathrm{BJD_{TDB}}$−2454833	T_{14} (hr)	Rp/R^* (%)	R_* ($R_\odot$)	T_{eff} (K)	R_P ($R_\oplus$)	S_{inc} ($S_\oplus$)	Notes
212496592.01	12.966	$2.85883^{+0.00039}_{-0.00038}$	$3347.0222^{+0.0047}_{-0.0053}$	$2.17^{+0.40}_{-0.29}$	$1.89^{+0.23}_{-0.20}$	0.86	5284	$1.77^{+0.22}_{-0.19}$	352	K2-191b (Mayo et al. 2018)
212521166.01	11.590	$13.8642^{+0.0011}_{-0.0011}$	$3357.3269^{+0.0028}_{-0.0027}$	$3.26^{+0.24}_{-0.18}$	$3.35^{+0.25}_{-0.21}$	0.72	4915	$2.62^{+0.20}_{-0.16}$	25.5	K2-110b (Osborn et al. 2017)
212554013.01	14.733	$3.588223^{+0.000046}_{-0.000045}$	$3348.97026^{+0.00046}_{-0.00047}$	$2.137^{+0.086}_{-0.073}$	$11.61^{+0.47}_{-0.70}$	0.95	5324	$12.01^{+0.65}_{-0.77}$	336	K2-127b (Dressing et al. 2017b)
212570977.01	13.928	$8.853181^{+0.000052}_{-0.000051}$	$3347.02423^{+0.00021}_{-0.00022}$	$4.192^{+0.029}_{-0.027}$	$15.33^{+0.22}_{-0.15}$	1.14	5774	$19.04^{+0.63}_{-0.62}$	183	…
212572439.01	12.835	$2.581446^{+0.000038}_{-0.000038}$	$3347.75306^{+0.00055}_{-0.00054}$	$1.81^{+0.23}_{-0.12}$	$6.17^{+0.67}_{-0.65}$	0.85	5124	$5.72^{+0.63}_{-0.60}$	344	Blend with 212572452
212572452.01	14.769	$2.581446^{+0.000019}_{-0.000020}$	$3347.75323^{+0.00030}_{-0.00028}$	$1.761^{+0.036}_{-0.039}$	$7.19^{+0.61}_{-0.50}$	0.67	4535	$5.23^{+0.46}_{-0.38}$	160	Blend with 212572439
212575828.01	15.508	$2.06033^{+0.00018}_{-0.00018}$	$3347.0331^{+0.0033}_{-0.0033}$	$1.55^{+0.27}_{-0.14}$	$3.71^{+0.38}_{-0.37}$	0.76	4949	$3.07^{+0.33}_{-0.32}$	364	…
212580872.01	13.047	$14.7881^{+0.0013}_{-0.0012}$	$3352.4604^{+0.0029}_{-0.0029}$	$4.34^{+0.74}_{-0.20}$	$3.70^{+0.24}_{-0.54}$	0.98	5586	$3.93^{+0.26}_{-0.57}$	60.8	K2-193b (Mayo et al. 2018)
212619190.01	12.788	$0.911861^{+0.000032}_{-0.000036}$	$3347.2783^{+0.0015}_{-0.0013}$	$0.772^{+0.121}_{-0.069}$	$2.33^{+0.23}_{-0.20}$	1.23	5765	$3.14^{+0.33}_{-0.29}$	4494	HD 119130
212628254.01	9.782	$16.9813^{+0.0022}_{-0.0022}$	$3347.2910^{+0.0044}_{-0.0046}$	$3.69^{+0.59}_{-0.31}$	$2.32^{+0.24}_{-0.24}$	1.08	5998	$2.74^{+0.29}_{-0.29}$	77.9	…
212628477.01	12.533	$15.42404^{+0.00081}_{-0.00097}$	$3347.7248^{+0.0020}_{-0.0019}$	$1.54^{+0.26}_{-0.23}$	$13.8^{+10.2}_{-1.4}$	1.39	5823	$21.0^{+15.4}_{-2.2}$	132	Grazing transit
212634172.01	14.831	$2.851770^{+0.000083}_{-0.000092}$	$3348.4657^{+0.0013}_{-0.0011}$	$0.721^{+0.140}_{-0.062}$	$7.27^{+0.98}_{-0.64}$	0.38	3585	$2.99^{+0.42}_{-0.30}$	25.4	…
212661144.01	13.595	$2.45875^{+0.00022}_{-0.00019}$	$3347.2747^{+0.0028}_{-0.0031}$	$1.10^{+0.29}_{-0.18}$	$3.10^{+0.41}_{-0.41}$	0.98	5647	$3.30^{+0.45}_{-0.44}$	698	…
212682254.01	13.565	$10.70070^{+0.00088}_{-0.00090}$	$3353.1746^{+0.0027}_{-0.0028}$	$3.23^{+0.31}_{-0.34}$	$4.74^{+2.05}_{-0.93}$	1.12	5936	$5.8^{+3.2}_{-1.8}$	148	…
212686205.01	12.256	$5.67623^{+0.00042}_{-0.00056}$	$3347.6471^{+0.0044}_{-0.0031}$	$1.45^{+0.21}_{-0.12}$	$2.05^{+0.20}_{-0.18}$	0.67	4566	$1.49^{+0.15}_{-0.13}$	57.1	K2-128b (Dressing et al. 2017b)
212686312.01	15.192	$0.7476280^{+0.0000027}_{-0.0000027}$	$3346.76330^{+0.00015}_{-0.00014}$	$1.434^{+0.079}_{-0.067}$	$45.4^{+10.8}_{-8.1}$	0.53	3904	$26.0^{+6.8}_{-5.1}$	335	Grazing transit
212689874.01	12.330	$15.8537^{+0.0013}_{-0.0013}$	$3359.2217^{+0.0024}_{-0.0023}$	$4.52^{+0.21}_{-0.15}$	$3.11^{+0.21}_{-0.12}$	0.98	5842	$3.32^{+0.23}_{-0.14}$	65.7	K2-195b (Mayo et al. 2018)
212689874.02	12.330	$28.4545^{+0.0034}_{-0.0034}$	$3349.1480^{+0.0044}_{-0.0041}$	$6.08^{+0.54}_{-0.40}$	$2.67^{+0.37}_{-0.21}$	0.98	5842	$2.85^{+0.39}_{-0.23}$	30.1	K2-195c (Mayo et al. 2018)
212697709.01	12.193	$3.951632^{+0.000030}_{-0.000030}$	$3349.48035^{+0.00029}_{-0.00029}$	$1.82^{+0.12}_{-0.10}$	$7.40^{+1.01}_{-0.57}$	1.09	5860	$8.77^{+1.18}_{-0.71}$	494	WASP-157, K2-41 (Močnik et al. 2016)
212707574.01	13.861	$1.12665^{+0.00018}_{-0.00014}$	$3346.9600^{+0.0047}_{-0.0067}$	$2.36^{+0.46}_{-0.28}$	$2.38^{+0.22}_{-0.25}$	1.63	5967	$4.24^{+0.48}_{-0.47}$	5618	…
212735333.01	11.977	$8.35812^{+0.00039}_{-0.00043}$	$3354.6901^{+0.0019}_{-0.0018}$	$3.30^{+0.16}_{-0.13}$	$2.63^{+0.13}_{-0.11}$	0.93	5642	$2.66^{+0.14}_{-0.12}$	121.8	K2-197b (Mayo et al. 2018)
212748535.01	13.582	$5.47826^{+0.00034}_{-0.00033}$	$3349.3152^{+0.0021}_{-0.0020}$	$1.53^{+0.21}_{-0.15}$	$3.51^{+0.33}_{-0.29}$	0.60	3971	$2.30^{+0.23}_{-0.20}$	30.2	…
212768333.01	16.825	$17.04518^{+0.00098}_{-0.00095}$	$3360.0516^{+0.0018}_{-0.0018}$	$3.65^{+0.25}_{-0.75}$	$4.24^{+0.64}_{-0.84}$	0.77	5232	$3.56^{+0.54}_{-0.70}$	27.2	K2-198b (Mayo et al. 2018)
212768333.02	16.825	$7.44957^{+0.00067}_{-0.00068}$	$3349.0808^{+0.0034}_{-0.0034}$	$2.86^{+0.56}_{-0.22}$	$2.80^{+0.29}_{-0.30}$	0.77	5232	$2.34^{+0.24}_{-0.25}$	81.9	Candidate from Pope et al. (2016)
212771557.01	13.950	$8.4902^{+0.0014}_{-0.0014}$	$3349.4717^{+0.0047}_{-0.0048}$	$2.55^{+0.32}_{-0.21}$	$2.56^{+0.26}_{-0.23}$	0.86	5530	$2.39^{+0.25}_{-0.22}$	99	…
212779563.01	9.945	$6.00123^{+0.00012}_{-0.00018}$	$3352.36041^{+0.00101}_{-0.00079}$	$1.272^{+0.102}_{-0.031}$	$2.73^{+0.11}_{-0.12}$	0.69	4688	$2.064^{+0.088}_{-0.097}$	62.5	Wolf 503 (Peterson et al. 2018)
212779596.01	11.930	$7.37416^{+0.00023}_{-0.00023}$	$3348.6147^{+0.0011}_{-0.0011}$	$2.361^{+0.128}_{-0.091}$	$4.02^{+0.25}_{-0.19}$	0.67	4772	$2.93^{+0.18}_{-0.14}$	48.2	K2-199b (Mayo et al. 2018)
212779596.02	11.930	$3.22575^{+0.00014}_{-0.00014}$	$3346.9032^{+0.0017}_{-0.0017}$	$1.872^{+0.151}_{-0.090}$	$2.58^{+0.16}_{-0.14}$	0.67	4772	$1.88^{+0.12}_{-0.10}$	145	K2-199c (Mayo et al. 2018)
212803289.01	11.014	$18.24605^{+0.00083}_{-0.00090}$	$3349.7141^{+0.0016}_{-0.0016}$	$10.905^{+0.085}_{-0.076}$	$3.738^{+0.075}_{-0.047}$	2.59	6560	$10.57^{+0.38}_{-0.35}$	422	K2-99b (Smith et al. 2017)
212813907.01	14.070	$6.72526^{+0.00031}_{-0.00033}$	$3350.5430^{+0.0016}_{-0.0016}$	$0.82^{+0.17}_{-0.13}$	$5.56^{+1.27}_{-0.59}$	0.79	5007	$4.79^{+1.10}_{-0.52}$	82.1	…
212870185.01	13.149	$6.11665^{+0.00044}_{-0.00044}$	$3347.9964^{+0.0027}_{-0.0026}$	$2.54^{+0.28}_{-0.18}$	$3.04^{+0.28}_{-0.25}$	1.12	5587	$3.73^{+0.36}_{-0.32}$	258	…
251554286.01	12.091	$15.46659^{+0.00066}_{-0.00064}$	$3356.8506^{+0.0011}_{-0.0012}$	$3.55^{+0.37}_{-0.42}$	$4.44^{+0.50}_{-0.80}$	0.98	5657	$4.73^{+0.56}_{-0.85}$	60.0	…
251582120.01	15.175	$0.509967^{+0.000055}_{-0.000051}$	$3346.9256^{+0.0029}_{-0.0043}$	$3.25^{+0.56}_{-0.59}$	$4.72^{+0.81}_{-0.44}$	1.25	5997	$6.49^{+1.18}_{-0.78}$	10946	…
251590700.01	13.302	$5.82105^{+0.00097}_{-0.00100}$	$3347.5528^{+0.0058}_{-0.0058}$	$6.1^{+3.3}_{-6.1}$	$6.40^{+0.78}_{-0.50}$	0.86	5247	$6.1^{+3.9}_{-3.8}$	138	Low $\rho_{*,\mathrm{circ}}$.

(This table is available in machine-readable form.)

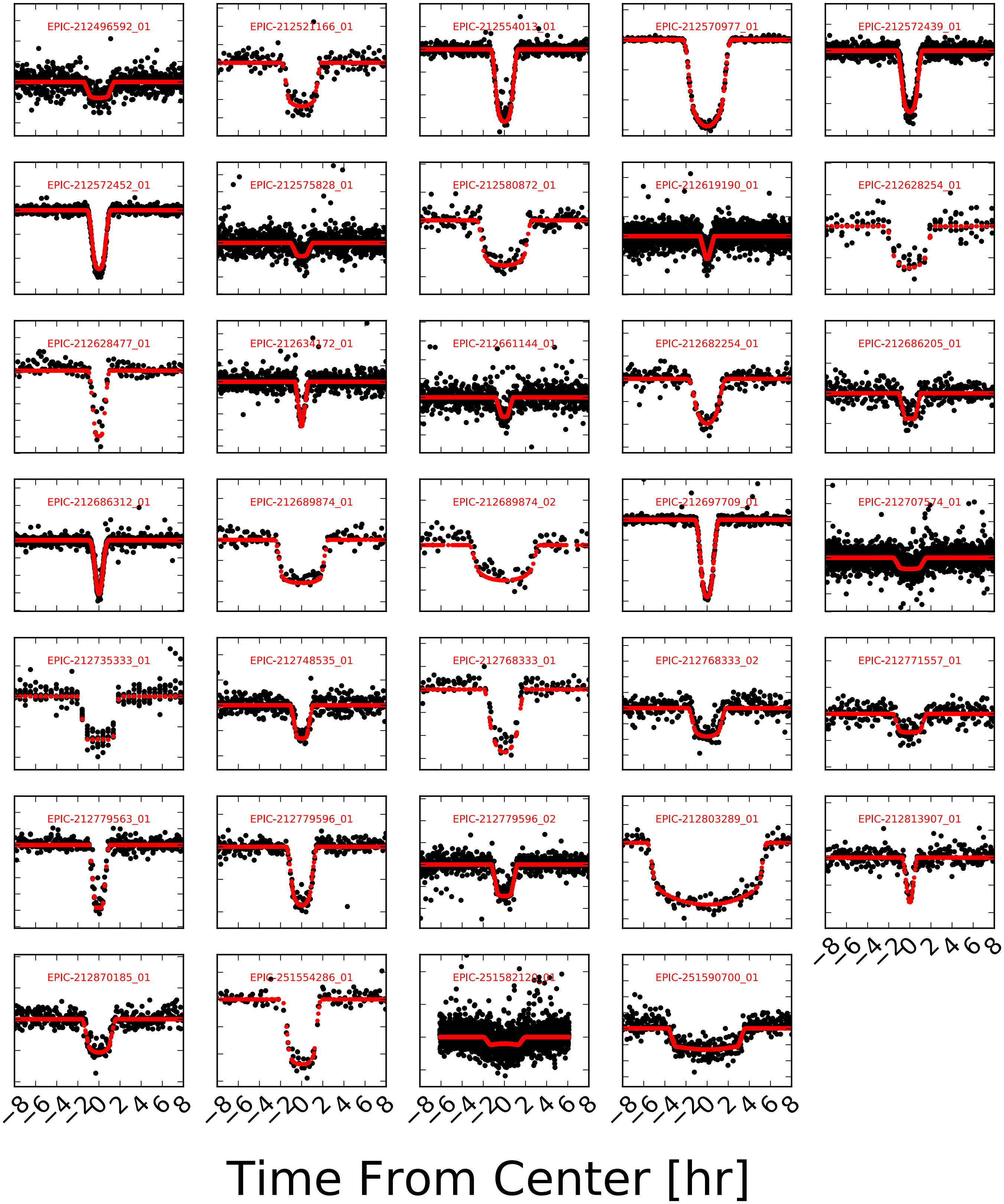

Figure 3. Phase-folded light curves of our 34 planet candidates, and their best-fit transit models. To show all transits, the vertical scale is different in each panel; system parameters are listed in Table 2.

212572439, 212580872, 212689874, 212697709, 212735333, 212779596, and 212803289. In a follow-up paper, Livingston et al. (2018, submitted) validated EPIC 212521166, 212554013, 212580872, 212689874, and 212779596. EPIC 212697709 remains a candidate in the latter paper with a false positive probability of 1.9%, but this planet was validated as WASP-157 (Močnik et al. 2016). Livingston et al. also found a sufficiently low FPP to validate EPIC 212803289

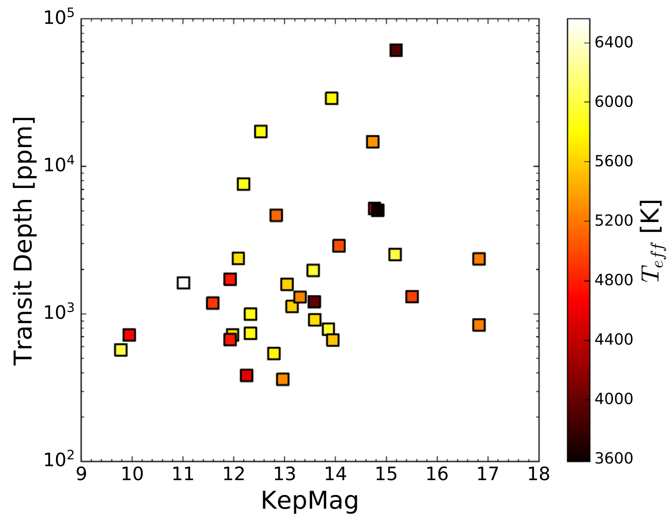

Figure 4. Transit depth and stellar magnitude for our planet candidates, as a function of stellar $T_{\rm eff}$ (color scale). The two brightest targets are Wolf 503 (EPIC 212779563) and HD 119130 (EPIC 212628254).

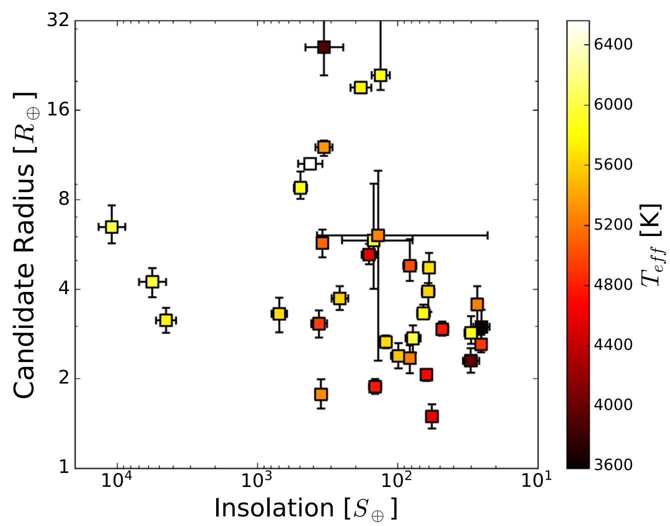

Figure 5. Candidate radius and incident insolation for our planet candidates, as a function of stellar $T_{\rm eff}$ (color scale).

and 212570977, but out of an abundance of caution they deemed these to be candidates because of their large radii (>10 $R_\oplus$). They also found EPIC 212572439 and 2127355333 to have very low FPPs but called these merely candidates because of an additional stellar source in the *K2* photometric aperture (E. Gonzales et al. 2018, in preparation).

As a further comparison, we calculated the ephemerides offsets of 11 of our C17 candidates with those derived from C6 data. To avoid possible biases that could arise from using different pipelines, we only compared those candidates with ephemerides reported by Livingston et al. (2018, submitted). Ephemerides for all 11 candidates are consistent at the 3σ level, with only three candidates disagreeing at the 2σ–3σ level (212570977.01, 212779596.01, and 212803289.01).

In summary: we identified 34 planet candidates in C17. Of those, 21 had been observed in C6 and all but one (212634172.01) had been previously identified in one or more previous surveys. Table 5 summarizes the overlap between the several samples, showing that no one combination of different methods, teams, thresholds, and other factors suffices to produce a fully complete planet candidate list—a result consistent with previous studies (e.g., Moutou et al. 2005).

6. Individual Systems

Below we discuss several interesting individual systems discovered by our C17 analysis. We separate these into several groups: potentially exciting discoveries warranting additional follow-up observations; more generic candidates nonetheless requiring some additional discussion; and objects that (though planet candidates) may be somewhat more likely to be non-planetary false positives.

1. 212779563 (Wolf 503, HIP 67285). This candidate planet's size of 2 $R_\oplus$ lies near the radius gap between sub-Neptunes and super-Earths (Fulton et al. 2017). The short period and nearby, bright star ($V = 10.3$, $H = 7.8$) could make this an excellent target for future RV and transmission spectroscopy. This system is described in more detail by Peterson et al. (2018).
2. 212628254 (HD 119130). This 2.7 $R_\oplus$ candidate orbits a $V = 9.9$, slightly evolved G star. It may also be a good RV target because of the planet's moderate size and bright host star.
3. 212689874 (K2-195). The transit light curve of this system shows possible spot-crossings, perhaps similar to those seen in CoRoT-29b (Cabrera et al. 2015).
4. 212813907. In addition to the transiting planet candidate reported here with $P = 6.7$ day, we see an obvious single transit with a depth of 1.8% centered at $\rm BJD_{TBD}$ = 2458213.82646 and with duration 0.66 day. The feature is well-defined, symmetric, and isolated in the light curve and thus is unlikely to be caused by stellar activity. The signal therefore points to a candidate transiting companion with a radius of $\sim 1\,R_{\rm Jup}$ and $P \approx 1000$ day. No corresponding transit was seen for this star during C6.
5. 212686205 (K2-128). (Dressing et al. 2017a) showed that this star is a K4 dwarf, despite its EPIC classification as a giant (Huber et al. 2016). The star exhibits semi-sinusoidal brightness variations that are likely due to starspots and stellar surface rotation, with a period of $P_{\rm rot} = 11.9$ days and amplitude of 0.018 mag. The position of the star in a rotation period–color diagram indicates an age similar to that of Praesepe (∼600–800 Myr).
6. 212768333. This candidate was validated as the single-planet K2-198b ($P = 17$ day) using data from C6 (Mayo et al. 2018), but our C17 data also reveal a second candidate with $P = 7.4$ day. These two candidates, plus a third ($P = 3.4$ day), were previously reported by Pope et al. (2016). The star has *K2* data available from Campaigns 6 and 17, making a search for additional transiting planets at longer orbital periods possible. The star shows periodic variability, which is likely due to rotation of the spotted surface. The inferred rotation period of 7.02 days and variability amplitude of 0.024 mag (from the 10th to 90th percentile) point to a young system age (Rebull et al. 2016, 2018), likely older than the Pleiades (125 Myr) but perhaps younger than or similar in age to Praesepe (∼600–800 Myr).
7. 212619190 and 212707574. These are both ultra-short-period (USP) planet candidates. While the signals are

Table 3
Eclipsing Binaries

EPIC	Kp (mag)	Epoch (BJD_{TDB})	P (day)	T_{14} (day)	$(R_P/R_*)^2$	Comments
212628098	13.259	2458180.89299	4.352574	0.067307	0.042013	…
212651213	10.796	2458180.35821	2.538338	0.144896	0.044374	V-shaped, large radius
212658818	12.070	2458180.48591	2.321117	0.066364	0.000868	blend because transit depth not consistent (not on target)
212757601	16.825	2458179.98367	1.017967	0.057751	0.012362	Jovian planet around small star? 7.7 $R_\oplus$
212769367	17.911	2458199.34193	20.225392	0.258937	0.021858	…
212769682	18.382	2458199.34810	20.230002	0.276014	0.041586	GAIA parallax <1 mas
212871068	18.318	2458182.72856	8.744013	0.183117	0.140517	
212884586	17.700	2458180.15931	2.882978	0.049651	0.011687	…
251810686	10.865	2458180.36230	2.537920	0.164611	0.059434	bad aperture; Rappaport et al. (2016)
212581374	10.292	2458180.14795	0.784498	0.157174	0.003875	…
212406350	13.923	2458179.72331	0.833679	0.083508	0.096367	…
212409856	13.446	2458179.83675	0.531704	0.078146	0.159770	…
212417656	12.745	2458179.74444	0.815627	0.136918	0.023504	…
212420474	13.442	2458179.83016	0.600579	0.066488	0.044711	…
212420510	14.632	2458179.82589	0.600656	0.077941	0.145720	contact
212421319	16.407	2458182.18746	5.528665	0.239914	0.014466	odd–even, wrong period
212421673	13.172	2458187.99492	28.248155	0.446599	0.003888	…
212426112	13.150	2458179.89122	1.530195	0.072284	0.035180	…
212428509	12.483	2458180.30248	2.667940	0.080248	0.007745	odd–even effect
212435964	14.080	2458193.11111	25.184817	0.201155	0.234665	…
212439709	14.352	2458180.15803	1.218136	0.066728	0.056980	contact, same as 1
212442107	15.821	2458180.02735	0.546059	0.074620	0.273964	…
212442408	11.778	2458180.41810	0.909676	0.123028	0.255280	…
212453473	13.957	2458181.97486	2.756129	0.150371	0.323040	…
212454161	15.225	2458180.76138	22.334245	0.610513	0.022610	…
212455982	14.140	2458180.67276	1.620017	0.242113	0.107147	…
212456583	13.429	2458182.17512	2.877393	0.164731	0.161885	…
212460623	9.086	2458179.98967	0.492488	0.086255	0.000156	…
212465919	15.159	2458180.05317	0.569619	0.081742	0.230555	contacting
212468149	14.814	2458179.86667	0.688366	0.059358	0.114282	…
212473154	8.980	2458181.23537	1.816975	0.083992	0.002040	…
212481328	13.090	2458179.55397	3.417361	0.105410	0.048337	…
212488008	10.633	2458189.49044	11.334688	0.070855	0.001533	…
212491978	14.025	2458179.95415	0.535811	0.062105	0.071267	contact, same as 1
212497267	12.282	2458182.01007	3.744355	0.180382	0.285638	…
212499716	13.748	2458180.06238	0.874745	0.035389	0.001790	…
212502064	9.671	2458179.70262	0.560679	0.088106	0.049133	contact
212504385	13.842	2458179.91896	0.826894	0.122608	0.249751	…
212509737	11.997	2458179.59591	2.343356	0.059597	0.008323	…
212511920	13.209	2458179.99753	0.572508	0.076707	0.097044	contact
212512022	16.643	2458179.89864	0.514313	0.124243	0.002423	contact
212518838	15.643	2458179.80762	0.651904	0.081742	0.198824	contact
212523277	17.547	2458179.75820	13.538932	0.114329	0.087378	…
212527975	13.708	2458179.68204	0.517780	0.081742	0.157632	contact
212530520	15.411	2458180.29465	0.808487	0.093941	0.118684	contact
212535959	13.803	2458190.36673	17.733194	0.292331	0.111249	…
212537106	12.982	2458181.36656	9.263450	0.273879	0.163254	…
212540174	14.869	2458179.57468	0.527054	0.040555	0.056895	contact
212540985	13.574	2458179.85092	0.548227	0.078714	0.035505	…
212541386	14.231	2458181.74987	3.630331	0.091115	0.074444	…
212545451	15.672	2458179.79113	1.133767	0.154570	0.450641	…
212545602	16.209	2458180.61219	1.756713	0.220238	0.670509	…
212546446	14.369	2458179.68614	0.655294	0.081742	0.133002	contact
212553193	15.314	2458179.68060	0.570422	0.079264	0.233006	…
212559866	11.864	2458184.00383	19.702223	0.383548	0.248986	…
212560752	12.839	2458179.91313	0.582783	0.081742	0.097117	…
212566769	13.331	2458189.13230	14.301229	0.323096	0.039127	…
212567829	18.076	2458180.10226	0.841796	0.119074	0.284914	…
212570257	12.523	2458179.69542	0.610230	0.055085	0.070548	secondary of contacting
212577519	14.234	2458180.54062	0.980712	0.077982	0.115798	contact
212579164	13.632	2458182.64844	18.155715	0.137503	0.230781	46 $R_\oplus$
212580081	18.233	2458180.41422	1.491851	0.088955	0.692969	35 $R_\oplus$
212580230	12.838	2458179.96998	0.563909	0.081742	0.367660	Contact

Table 3
(Continued)

EPIC	Kp (mag)	Epoch (BJD_{TDB})	P (day)	T_{14} (day)	$(R_P/R_*)^2$	Comments
212586717	13.875	2458181.71797	4.295939	0.087219	0.012705	⋯
212601505	14.486	2458179.96618	0.724453	0.035719	0.020973	⋯
212609851	15.164	2458179.82750	0.642765	0.057191	0.223025	⋯
212611243	14.163	2458179.94634	0.726623	0.077036	0.097420	⋯
212612033	18.300	2458179.98494	1.049595	0.091376	0.022397	⋯
212613128	13.861	2458180.19045	0.759210	0.070657	0.213789	⋯
212615099	15.660	2458192.20124	16.397313	0.105083	0.122559	⋯
212617879	12.316	2458179.84646	2.210766	0.153759	0.142075	⋯
212627712	13.265	2458186.21980	19.913432	0.145782	0.165860	107 $R_\oplus$
212629807	15.143	2458179.90970	0.501935	0.081742	0.206343	contact
212631911	15.546	2458179.98736	0.520852	0.078445	0.333555	⋯
212634594	15.202	2458184.28069	6.401944	0.145015	0.212873	⋯
212641218	14.993	2458179.98311	1.049606	0.076901	0.001691	⋯
212644753	9.422	2458179.97694	1.049846	0.097062	0.041131	⋯
212651213	10.796	2458191.53766	13.196894	0.199239	0.010896	Rappaport et al. (2016)
212651234	11.139	2458180.35324	2.538731	0.123252	0.008702	Rappaport et al. (2016); 30.5 $R_\oplus$
212652663	14.819	2458180.77106	1.669747	0.102005	0.228074	⋯
212654750	13.917	2458179.88743	0.529294	0.081742	0.413695	contact
212657659	17.470	2458180.01607	0.546679	0.055120	0.014074	contact
212666524	14.293	2458179.90638	0.670516	0.081742	0.121268	⋯
212666639	15.366	2458179.54065	0.541019	0.079310	0.301795	contact
212667298	12.902	2458179.54657	0.606965	0.081742	0.435121	contact
212671857	13.697	2458180.24217	0.727391	0.068894	0.139981	⋯
212679798	14.846	2458180.12895	1.834750	0.073377	0.033351	⋯
212686943	13.774	2458181.02088	1.578709	0.165925	0.064449	⋯
212687040	13.475	2458180.27371	1.852983	0.106111	0.205153	⋯
212689699	17.593	2458180.07219	0.518523	0.130845	0.013282	contact
212690087	14.746	2458180.09903	0.786832	0.114912	0.042193	⋯
212691727	12.657	2458184.17922	12.862016	0.201678	0.050839	⋯
212695400	15.403	2458180.22806	0.848459	0.065686	0.215148	⋯
212697951	12.582	2458180.27911	1.912398	0.114449	0.259949	star spot causes modulation
212701118	12.691	2458179.72465	2.434027	0.144225	0.661748	⋯
212702889	14.558	2458179.93264	0.631071	0.056983	0.052287	⋯
212705192	11.728	2458181.41157	2.268360	0.048411	0.005948	odd–even effect, double-lined
212705508	14.415	2458180.05063	0.603816	0.044304	0.003131	⋯
212707624	13.179	2458182.00981	3.604588	0.207304	0.106715	⋯
212708296	15.906	2458180.26857	0.803247	0.100811	0.466097	⋯
212708783	10.386	2458179.95230	2.253755	0.142294	0.118586	⋯
212710571	17.458	2458179.95368	2.253558	0.104992	0.012538	⋯
212712870	15.304	2458179.96661	0.494226	0.069594	0.249001	⋯
212716448	18.478	2458180.01069	0.546752	0.058736	0.062706	same as 1
212723069	14.817	2458186.05758	11.495130	0.232389	0.037574	⋯
212723581	15.961	2458180.00972	0.600845	0.066764	0.124436	same signal as 1
212733831	14.786	2458179.70777	0.732994	0.081742	0.117807	⋯
212734205	17.588	2458181.12287	4.965604	0.493681	0.397380	⋯
212737890	15.875	2458179.84702	0.880552	0.105444	0.127097	⋯
212740148	13.996	2458180.15919	0.741042	0.030996	0.011375	⋯
212741343	15.933	2458180.05956	0.580501	0.054682	0.100483	contact
212746282	12.518	2458179.85030	0.595119	0.081742	0.093743	contact
212747879	15.717	2458179.97540	0.705760	0.081742	0.331363	⋯
212748031	15.678	2458180.36357	0.887395	0.037098	0.005056	⋯
212751079	13.700	2458179.62410	0.595131	0.142401	0.264229	⋯
212751916	13.890	2458180.64439	15.715606	0.097758	0.004367	⋯
212759326	13.892	2458182.52706	3.376283	0.117698	0.076310	⋯
212770429	11.153	2458199.35119	20.225506	0.342386	0.210533	75 $R_\oplus$
212771092	17.554	2458180.04000	0.613816	0.081742	0.513770	⋯
212771522	14.105	2458180.36577	0.964855	0.036899	0.002141	⋯
212773272	14.965	2458182.45629	4.681890	0.080497	0.043560	⋯
212773309	11.391	2458182.45642	4.681764	0.093543	0.074791	⋯
212781530	15.601	2458180.03084	0.574416	0.081742	0.518721	contact
212781903	13.952	2458179.93093	0.516312	0.081742	0.057071	⋯
212786474	14.472	2458179.57656	9.271273	0.151254	0.429256	⋯
212789681	13.740	2458179.55289	0.497467	0.116872	0.000516	contact

Table 3
(Continued)

EPIC	Kp (mag)	Epoch (BJD_{TDB})	P (day)	T_{14} (day)	$(R_P/R_*)^2$	Comments
212796590	16.506	2458179.97098	0.555792	0.144363	0.009497	contact
212801119	12.771	2458180.11071	0.591442	0.045596	0.019034	…
212801667	11.911	2458186.41163	23.274142	0.214440	0.075892	…
212805198	14.422	2458180.96489	3.228788	0.086784	0.079089	…
212812349	13.712	2458185.62953	8.167374	0.174965	0.069996	…
212814517	15.896	2458179.76158	0.624914	0.079529	0.314121	…
212822491	11.078	2458186.08017	14.321271	0.265478	0.171877	…
212824416	16.638	2458179.85284	0.590807	0.057018	0.134113	contact EB; secondary
212826509	16.297	2458180.41915	0.988762	0.113296	0.311666	…
212827749	13.358	2458185.76643	11.345548	0.187133	0.207902	…
212828964	16.170	2458179.90943	0.646399	0.142256	0.001916	contact
212834326	15.554	2458180.10438	0.780977	0.079370	0.242254	…
212837770	16.663	2458180.22595	0.850575	0.064098	0.263615	…
212839815	12.874	2458180.59961	4.441165	0.198630	0.037661	…
212842049	16.894	2458181.48623	3.289052	0.066265	0.062749	…
212842366	12.081	2458179.58419	0.543994	0.059710	0.018823	…
212854191	12.566	2458180.39309	0.868807	0.099834	0.046954	contact
212864075	11.826	2458180.11467	0.729410	0.071462	0.015258	…
212866286	12.702	2458180.51003	4.717350	0.245227	0.178060	…
212869892	12.392	2458179.99254	0.814852	0.057258	0.008050	…
212872008	14.464	2458180.76477	1.311925	0.107024	0.102602	…
212872519	18.895	2458180.02866	1.361929	0.188677	0.316683	…
212878430	18.479	2458179.64683	0.511345	0.081742	0.086995	contact
212884295	16.098	2458180.05753	0.632894	0.082281	0.151918	contact
212885442	15.582	2458179.58563	0.626888	0.081742	0.192118	…
251505087	16.021	2458180.01374	0.744603	0.080170	0.204046	…
251505480	18.300	2458179.54528	0.622504	0.080448	0.117676	contact
251505499	9.619	2458179.54539	0.622507	0.081742	0.278995	contact
251508456	15.216	2458179.90526	0.774116	0.142628	0.773576	…
251508975	16.979	2458179.93148	0.583320	0.081742	0.142980	…
251512942	14.262	2458179.54192	0.546855	0.081742	0.249001	contacting
251523672	16.201	2458179.84407	0.594784	0.043602	0.153440	contact
251524025	16.805	2458179.79873	0.638134	0.073617	0.386702	…
251539042	15.597	2458179.53378	0.561767	0.076747	0.249001	…
251543556	13.596	2458179.96760	0.498006	0.049089	0.018157	…
251551459	16.526	2458179.76260	0.938771	0.083508	0.235088	…
251566115	12.519	2458182.48929	11.850868	0.127530	0.072908	…
251567015	16.442	2458179.68328	0.558434	0.073032	0.111879	contact
251571270	17.339	2458179.61675	0.645707	0.048994	0.425897	…
251575183	18.642	2458179.89846	0.515838	0.070330	0.116968	…
251600179	17.983	2458179.74495	0.668258	0.055939	0.071262	…
251606815	15.059	2458179.53572	0.514761	0.081742	0.405411	…
251612064	15.053	2458179.72566	0.519174	0.081742	0.367738	…
251613109	17.532	2458180.09242	0.603096	0.075259	0.282421	…
251628925	12.632	2458197.00901	23.932888	0.374788	0.073781	…
251809768	18.310	2458182.00880	3.744813	0.132943	0.027276	…
251809787	16.978	2458180.14621	0.874333	0.111146	0.174670	…
251809799	18.088	2458179.77296	0.929420	0.101403	0.209458	…
251809801	18.209	2458180.14037	5.424922	0.239628	0.047817	…
251809804	18.366	2458181.02178	3.044908	0.394803	0.336826	…
251809805	18.431	2458179.87263	0.493215	0.072998	0.260563	contact
251809808	18.531	2458179.64709	0.986293	0.204333	0.341796	…
251809809	18.694	2458179.63921	0.543684	0.081742	0.091127	contact
251809830	19.404	2458180.01339	0.746323	0.081742	0.313398	…
251809968	19.390	2458179.54579	0.622505	0.081742	0.185758	…
251810686	10.865	2458186.24598	13.191424	0.151051	0.012218	quintuple system, Rappaport et al. (2016)
251539584	10.763	2458179.55118	1.088222	0.045042	0.000625	SB2, blend with 251539609
251539609	11.016	2458179.55151	1.088213	0.044667	0.000624	SB2, blend with 251539584

(This table is available in machine-readable form.)

Table 4
Other Periodic Variables

EPIC	*Kp* (mag)	*P* (day)	Comments
212404864	17.754	0.583854	⋯
212416035	18.061	0.650274	⋯
212424629	16.018	0.651446	⋯
212424861	17.877	0.651436	⋯
212425817	16.684	0.715986	RR Lyrae
212426904	15.519	1.559636	⋯
212429810	9.835	1.751454	⋯
212431975	12.460	0.560643	⋯
212433098	14.338	0.755435	⋯
212433328	14.893	1.155617	⋯
212439709	14.352	0.609047	contact?
212440192	16.146	0.531711	⋯
212441076	14.847	0.528502	⋯
212443701	16.789	0.683153	⋯
212449290	16.309	0.847446	⋯
212449840	14.091	0.558064	⋯
212450261	12.888	3.746695	⋯
212453596	16.109	0.595544	⋯
212460039	9.020	0.571204	⋯
212461484	7.976	2.268343	⋯
212463213	14.966	0.644204	⋯
212467265	16.591	0.617039	⋯
212469922	12.509	0.810722	⋯
212470542	14.767	0.501587	⋯
212470959	16.904	0.909599	⋯
212475454	14.591	0.495057	⋯
212476230	14.065	0.909933	⋯
212476743	16.906	0.626211	⋯
212476895	12.756	0.806344	⋯
212478962	15.411	0.609325	⋯
212479061	18.334	0.491113	⋯
212481276	14.791	0.560738	⋯
212491978	14.025	0.535797	⋯
212492961	12.942	0.746502	⋯
212503342	8.324	0.501263	⋯
212504059	11.601	0.505806	⋯
212506921	16.857	0.537091	⋯
212506981	18.107	0.560708	⋯
212519490	12.859	0.553239	⋯
212520127	16.474	0.787684	⋯
212529254	15.890	1.224833	⋯
212530684	17.050	0.505286	large OOT amplitude
212534342	17.713	0.617741	⋯
212537690	16.567	0.605773	⋯
212540092	17.920	0.558487	⋯
212542474	12.033	0.526188	⋯
212551424	13.270	0.634884	⋯
212555590	14.733	0.636359	⋯
212560096	14.764	0.599002	⋯
212561206	15.129	0.615971	⋯
212562145	14.856	0.728760	⋯
212564937	14.129	0.506676	⋯
212570257	12.523	0.610247	⋯
212575000	16.145	0.735286	⋯
212575799	15.277	0.616666	⋯
212575959	12.439	0.670392	⋯
212578200	13.144	1.131015	⋯
212589990	12.178	0.504842	⋯
212594525	15.888	0.762575	⋯
212597328	18.187	0.658850	RR Lyrae
212601233	14.997	0.636031	⋯
212603282	12.328	0.696329	⋯
212603536	11.933	0.720349	⋯

Table 4
(Continued)

EPIC	*Kp* (mag)	*P* (day)	Comments
212603999	15.443	0.502387	RR Lyrae
212609833	16.543	0.570110	⋯
212612729	14.534	0.904916	⋯
212617685	13.406	0.594009	⋯
212619206	15.542	0.687767	⋯
212620826	13.616	0.789620	⋯
212621423	14.951	0.817041	⋯
212628986	15.071	1.428411	⋯
212631286	13.236	0.525008	⋯
212631414	13.022	0.525005	⋯
212631757	16.082	0.175266	⋯
212636050	15.543	0.630885	⋯
212639395	16.928	0.591004	⋯
212639932	16.316	0.619463	⋯
212640806	15.889	0.510041	⋯
212642195	14.144	0.629391	⋯
212644219	16.174	0.622971	⋯
212648945	13.771	0.750334	⋯
212659834	11.665	0.546711	⋯
212666537	16.115	0.494617	⋯
212669531	13.967	0.606174	⋯
212672666	16.536	0.520714	⋯
212674862	15.842	0.675189	⋯
212676658	10.640	0.532304	⋯
212699845	17.389	0.616183	⋯
212703179	11.251	0.673494	⋯
212704410	10.588	0.762124	⋯
212706992	14.171	0.573939	⋯
212711185	15.760	0.676885	⋯
212711671	14.949	0.545729	⋯
212715425	14.822	0.542155	⋯
212716271	15.192	0.546693	⋯
212716448	18.478	0.546688	⋯
212716631	18.970	0.573803	⋯
212717166	16.262	0.586327	⋯
212718800	13.631	0.650108	⋯
212719030	15.126	1.349336	⋯
212720186	16.530	0.626749	⋯
212722087	12.587	0.546000	⋯
212722872	14.345	0.692869	⋯
212723581	15.961	0.600851	⋯
212730754	17.858	0.587020	⋯
212732420	13.805	0.546859	⋯
212733211	16.553	0.592465	⋯
212735753	17.112	0.611941	⋯
212736684	18.155	0.548902	⋯
212742333	18.142	0.582756	⋯
212749368	16.551	0.630246	⋯
212755404	13.810	0.758773	⋯
212760038	11.199	0.598949	⋯
212766036	16.427	1.128395	⋯
212775050	16.256	0.633570	⋯
212775136	13.127	0.520693	⋯
212783579	13.453	0.623693	⋯
212784817	15.000	0.735008	⋯
212785152	15.295	0.688545	⋯
212791551	19.214	0.720158	⋯
212791701	16.337	0.533695	⋯
212793961	12.154	0.633511	⋯
212794694	17.778	0.505073	⋯
212794999	16.022	0.602511	⋯
212795516	17.724	0.613296	⋯
212798939	16.823	0.507892	⋯

Table 4
(Continued)

EPIC	Kp (mag)	P (day)	Comments
212801998	15.450	0.517430	⋯
212808944	13.005	0.670074	⋯
212812050	13.882	0.575880	⋯
212814000	14.807	0.561011	⋯
212814419	18.297	0.625019	⋯
212814441	14.201	0.783737	⋯
212818222	16.219	0.584496	⋯
212818294	16.194	0.829784	⋯
212820594	14.665	0.530704	⋯
212821516	11.946	0.508947	⋯
212824416	16.638	0.590808	⋯
212827294	16.930	0.559323	⋯
212828640	14.934	0.592274	⋯
212828933	14.283	0.716170	⋯
212829102	12.264	0.500330	⋯
212829130	16.467	0.646563	⋯
212829294	17.079	0.754500	⋯
212830414	16.810	0.571236	⋯
212831062	15.007	0.705463	⋯
212831234	13.076	0.649151	⋯
212833004	9.158	0.543036	⋯
212835551	12.676	0.562135	⋯
212835780	16.332	1.673125	⋯
212847938	15.743	0.607034	⋯
212853330	16.549	0.587536	⋯
212862638	15.191	0.497067	⋯
212867164	17.189	0.572633	⋯
212869088	17.220	0.505407	⋯
212870977	14.714	0.507252	⋯
212873395	12.808	0.605284	⋯
212879205	12.829	0.649341	⋯
212879653	11.576	0.517211	⋯
212881555	17.099	0.545534	⋯
212882485	15.839	0.624794	⋯
212882871	19.921	0.612855	⋯
212883764	15.503	0.668488	⋯
212884307	13.143	0.583500	⋯
229228086	17.360	0.620306	⋯
229228087	17.630	0.602832	⋯
229228091	18.240	0.600837	⋯
229228112	17.940	0.591997	⋯
229228121	17.770	0.574762	⋯
251501619	14.964	0.580914	⋯
251502557	13.714	0.679484	⋯
251504831	17.611	0.622515	⋯
251504891	9.777	0.528140	⋯
251505259	17.675	0.622474	⋯
251509348	16.172	0.623298	⋯
251517127	18.061	0.714932	⋯
251519864	11.446	1.275710	⋯
251520093	18.417	0.540185	⋯
251523672	16.201	0.594779	⋯
251526009	18.424	0.672721	⋯
251529654	16.234	0.521895	⋯
251530257	17.204	0.641235	⋯
251540409	16.770	0.537995	⋯
251554210	16.357	0.509245	⋯
251564868	18.244	0.494339	⋯
251566981	11.096	0.518554	⋯
251568443	14.911	0.714645	⋯
251569406	14.271	0.670480	⋯
251574051	13.248	2.206687	⋯
251578582	11.275	7.120210	⋯
251579007	14.922	0.629344	⋯
251583296	17.090	0.549769	⋯
251583388	14.011	0.950893	⋯
251585662	19.180	0.646642	⋯
251590688	12.081	0.710497	⋯
251596880	10.890	2.633147	⋯
251599500	15.101	0.571171	⋯
251602987	17.865	0.688673	⋯
251608983	12.951	0.934933	⋯
251611842	12.691	0.518191	⋯
251612403	15.626	0.698081	⋯
251613106	17.050	0.717477	⋯
251615995	14.797	0.561389	⋯
251809762	17.770	0.574708	⋯
251809767	18.290	0.609255	⋯
251809792	17.702	0.582034	⋯
251809793	17.830	0.535073	⋯
251809794	17.837	0.514385	⋯
251809800	18.158	0.644357	⋯
251809802	18.232	0.565049	⋯
251809803	18.271	0.538007	⋯
251809807	18.499	0.605395	⋯
251809812	18.954	0.615473	⋯
251809817	19.009	0.598227	⋯
251809820	19.110	0.573687	⋯
251809824	19.182	0.709409	⋯
251809836	19.611	0.591795	⋯
251809865	20.310	0.669433	⋯
251810875	18.667	0.643312	⋯
251811189	18.981	0.560705	⋯
251811486	19.100	0.798840	⋯
251811829	19.187	0.651565	⋯
251809821	19.110	0.610251	⋯

(This table is available in machine-readable form.)

convincing, the inferred sizes we report here are larger than those of typical USPs (Winn et al. 2018).

The following planet candidates seem reliable but warrant some additional discussion.

1. 212748535. We originally identified this candidate as a signal associated with EPIC 212748598 ($Kp = 17.4$ mag). This faint source is classified as a galaxy by The 2dF Galaxy Redshift Survey (Colless et al. 2001) and appears galaxy-like in Pan-Starrs multicolor imaging (A. Rest 2018, private communication). We conclude that EPIC 212748598 is a galaxy despite its designation as "STAR" in EPIC. *Gaia* DR2 shows a brighter, stellar source with $\Delta G = 5.4$ mag within our *K2* aperture and $20''$ away. This brighter star is EPIC 212748535, which *Gaia* shows to be a K dwarf ($T_{\rm eff} = 3800$ K, $R_* = 0.67\ R_\odot$) and which dominates the flux in our *K2* photometric aperture. We conclude that the brighter source, EPIC 212748535, is the true host of the observed $\sim$1 mmag transit. The galaxy will dilute the observed transit by roughly 1%, much less than the uncertainty on the transit depth and candidate radius.

Table 5
Our C17 Candidates Observed in C6

Candidate	C6	Po16	Ma18	Pe18	Li18	Name	Validation Reference/Note
212496592.01	Y	PC	VP	N	N	K2-191b	Mayo et al. (2018)
212521166.01	Y	PC	VP	PC	VP	K2-110b	Osborn et al. (2017)
212554013.01	Y	PC	N	PC	VP	K2-127b	Dressing et al. (2017b)
212570977.01	Y	PC	N	PC	PC	…	…
212572439.01	Y	PC	N	PC	PC	…	Blend with 212572452.
212572452.01	Y	PC	N	N	PC	…	Blend with 212572439.
212575828.01	Y	PC	N	N	N	…	…
212580872.01	Y	PC	VP	PC	VP	K2-193	Mayo et al. (2018)
212634172.01	Y	N	N	N	N	…	…
212661144.01	Y	PC	N	N	N	…	…
212686205.01	Y	N	VP	N	N	K2-128b	Dressing et al. (2017b)
212689874.01	Y	PC	VP	PC	VP	K2-195b	Mayo et al. (2018)
212689874.02	Y	PC	VP	PC	VP	K2-195c	Mayo et al. (2018)
212697709.01	Y	PC	VP	PC	PC	WASP-157b	Močnik et al. (2016)
212735333.01	Y	PC	VP	PC	PC	K2-197b	Mayo et al. (2018)
212768333.01	Y	PC	VP	N	N	K2-198b	Mayo et al. (2018)
212768333.02	Y	PC	N	N	N		…
212779596.01	Y	PC	VP	PC	VP	K2-199b	Mayo et al. (2018)
212779596.02	Y	PC	VP	PC	VP	K2-199c	Mayo et al. (2018)
212803289.01	Y	PC	VP	PC	PC	K2-99b	Smith et al. (2017)
212813907.01	Y	PC	N	N	N	…	…

Notes. VP (validated planet), PC (planet candidate), N (not identified).
References. Po16 (Pope et al. 2016), Ma18 (Mayo et al. 2018), Pe18 (Petigura et al. 2018), Li18 (Livingston et al. 2018, submitted).

2. 212682254: This star has a candidate with $R_C = 6\,R_\oplus$ and $P = 10.7$ day, and also shows photometric variability due to starspots, with an amplitude of 0.019 mag (again measured from the 10th to 90th percentile) and an inferred rotation period of 9.45 days. The rotation period and color place the star near the slowly rotating I-sequence of Praesepe members (Barnes 2007), indicating an age similar to that of that cluster (~600–800 Myr).
3. 212572439 and 212572452. Our analysis independently identified two candidates with the same periods around these adjacent stars (separated by 6″ and with consistent *Gaia* parallaxes). A transit-like signal from the blend of these two sources has also been identified in previous works (Dressing et al. 2017b; Petigura et al. 2018, Livingston et al. 2018, submitted; E. Gonzales et al. 2018, in preparation), and both signals were identified (though the blend went unremarked) by Pope et al. (2016). Based on our inferred stellar and planetary properties, this signal could still be a transiting planet regardless of which of these two stars it orbits; we thus retain both signals as planet candidates. Additional follow-up will be required to identify which object is the transit host.

Finally, the objects below pass our criteria as planet candidates but show warning signs hinting that they may be non-planetary:

1. 251590700. This source has no *Gaia* DR2 parallax, so the derived stellar parameters are somewhat less certain. The parallax measurement is presumably lacking because of an enormous amount of excess noise in the five-parameter *Gaia* solution (`astrometric_excess_noise_sig` = 64781), suggesting the possibility that the star is a binary. Our transit fit implies a stellar density (assuming a circular orbit; Seager & Mallén-Ornelas 2003) of $\rho_{*,\rm circ} = 0.0033^{+0.0005}_{-0.0003}$ g cm^{-1}, implying either a highly eccentric orbit or a false positive caused by an eclipsed, low-density giant star.
2. 251582120. We originally identified this event as a signal around EPIC 251581990, a faint ($Kp = 18.5$ mag) source listed as an "EXTENDED" (i.e., non-stellar) object in EPIC. Our aperture for this faint target enclosed another nearby brighter stellar source, EPIC 251582120 ($Kp = 15.2$ mag), whose flux dominates our light curve. Our light curve fit for this brighter source implies $\rho_{*,\rm circ} = 0.165 \pm 0.055$ g cm^{-1}, mildly inconsistent with our `isochrones`+*Gaia*-derived stellar density of 0.79 ± 0.20 g cm^{-1}. The crowded aperture and mismatch in stellar densities hint that this planet candidate may be less reliable, though the mismatch could also indicate an eccentric orbit.
3. 212686312. This signal is both deep (6%) and V-shaped, indicating a grazing transit. Combined with the very short orbital period and the inferred companion radius presented here of $26\,R_\oplus$, the planetary nature of the signal is doubtful.
4. 212628477. This star is rapidly rotating, with a period of 2.685 days and a variability amplitude of 0.045 mag. The star's rapid rotation combined with its color suggest an age younger than that of the Pleiades (Rebull et al. 2016). The rotation period is clearly distinct from the much longer period of the planet candidate ($P = 15.4$ day), but there are several warning signs for this candidate: the transits are grazing so the inferred companion is large ($21.0^{+15.4}_{-2.2}\,R_\oplus$); *Gaia* DR2 reports a highly uncertain radial velocity of 20.98 ± 19.55 km s^{-1}, perhaps indicative of RV variability; and the TRES spectrum shows a probable shoulder in the cross-correlation function indicating a double-lined spectrum (see Table 1).

Nonetheless this remains a planet candidate because it meets the current *TESS* criteria for planet candidates.

5. 251539584 and 251539609. These two stars are both spectroscopic binaries. Both showed candidate transit signals with the same transit ephemeris ($P = 1.09$ day). The stars are roughly equal in brightness ($\Delta Kp = 0.2$ mag), are separated by roughly 14″, and are both are contained in the photometric aperture applied to the other. The two stars are apparently associated and co-moving, based on their kinematics from *Gaia* DR2. The combined light curve is variable, indicating a rotation period of 4.34 days and amplitude of 0.002 mag (though the true amplitude must be larger because of flux dilution from the companion). TRES spectroscopy shows that both EPIC sources are short-period double-lined spectroscopic binaries (see Table 1), so we list these systems as candidate EBs.

7. Discussion and Conclusion

From ∼34,000 stars observed in *K2*'s most recent field, Campaign 17, we identified 1274 transit-like events. Among these, we find 34 planet candidates (Table 2), 184 eclipsing binaries (Table 3), and 222 other periodic variables (Table 4). Because C17 was observed in "forward-facing" mode by *K2* in its Earth-trailing orbit, these targets can be immediately observed before the ecliptic field sets for the season. Many of these objects were also observed by *K2* during C6, offering a rare opportunity to study the same systems over a 1000 day timespan. Multiple observations of the same field will be commonplace when *TESS* begins near-continuous observations of the ecliptic poles, which will substantially increase that survey's sensitivity to long-period planets. Though beyond the scope of this work, a comprehensive transit search in C6+C17 (or C5+C16) would probe a single, narrow range of orbital periods from 880 to 1030 day (and harmonics of these periods).

We evaluated the overlap between our C17 planet candidates and those observed in C6 by several earlier planet surveys, finding again that *K2* efforts have substantially different completeness (Crossfield et al. 2016; Mayo et al. 2018). The C6 catalog of Pope et al. (2016) overlaps most closely with our C17 candidate list, indicating that that sample has either a high degree of completeness or (at worst) a very similar set of biases to that of our sample. Unfortunately, the different samples and data quality between the calibrated C6 data and our use of C17's raw cadence data precludes any conclusions about false positive rates in these surveys. Nonetheless, the generally incomplete overlap between the candidate lists of different surveys lends support to the *TESS* science plan to use two independent pipelines, SPOC and QLP, to minimize the chances of interesting planet candidates passing unnoticed.

In this work we focus on the search for new transiting planet candidates, whose parameters are summarized in Table 2. We find several candidates that have sizes $<4\,R_\oplus$ and orbit stars with $Kp \lesssim 10$, indicating that these are good RV targets. The most interesting are Wolf 503 (EPIC 212779563.01; see Peterson et al. 2018, submitted) and HD 119130 (EPIC 212628254.01). If found by *TESS*, such planet candidates would be ideal targets for fulfilling its prime science goal of contributing to the measured masses of 50 small planets.

Several other planet candidate discoveries highlight potentially intriguing dynamical and/or multi-body systems. We see a single, deep transit around EPIC 212813907, which also hosts a 6 day planet candidate, suggesting a Jupiter-sized companion on a long-period orbit. We also identify a candidate planet in each of two possible binary systems (EPIC 251539584 & 251539609, and EPIC 212572439 & 212572452).

In conclusion, *K2*'s rapid data releases for its recent campaigns have facilitated quick identification of many interesting astrophysical phenomena in time for immediate ground-based follow-up. This approach is qualitatively the same as that planned for *TESS*. In this C17 exercise, our *TESS*-like and *K2*-like vetting approaches both yielded the same set of planet candidates. This result validates the results derived from similar, past analyses of *K2* and also demonstrates that the team members soon to be examining *TESS* data have the tools and expertise necessary for a successful mission. After four years *Kepler* yielded to *K2*; another four years on, in Olympic fashion, *K2* will likewise pass the baton to *TESS* to continue building on the great legacy of exoplanet exploration.

We thank the anonymous referee for useful comments that improved the quality of this paper. We thank A. Rest for discussions about the nature of EPIC 212748598. I.J.M.C. acknowledges support from NASA through K2GO grant 80NSSC18K0308 and from NSF through grant AST-1824644. Part of this research was carried out at the Jet Propulsion Laboratory, California Institute of Technology, under a contract with the National Aeronautics and Space Administration. T.J.D. acknowledges support from the JPL Exoplanetary Science Initiative This paper includes data collected by the *Kepler* mission. Funding for the *Kepler* mission is provided by the NASA Science Mission directorate. Some of the data presented in this paper were obtained from the Mikulski Archive for Space Telescopes (MAST). STScI is operated by the Association of Universities for Research in Astronomy, Inc., under NASA contract NAS5–26555. Support for MAST for non-*HST* data is provided by the NASA Office of Space Science via grant NNX13AC07G and by other grants and contracts. This research has made use of the Exoplanet Follow-up Observing Program (ExoFOP), which is operated by the California Institute of Technology, under contract with the National Aeronautics and Space Administration.

Facilities: Kepler, *K2*, FLWO:1.5 m (TRES), Keck:I (HIRES), APF (Levy).

ORCID iDs

Trevor David https://orcid.org/0000-0001-6534-6246
Samuel N. Quinn https://orcid.org/0000-0002-8964-8377
Chelsea Huang https://orcid.org/0000-0003-0918-7484
Liang Yu https://orcid.org/0000-0003-1667-5427
Karen A. Collins https://orcid.org/0000-0001-6588-9574
Benjamin J. Fulton https://orcid.org/0000-0003-3504-5316
Allyson Bieryla https://orcid.org/0000-0001-6637-5401
Joshua E. Schlieder https://orcid.org/0000-0001-5347-7062
Molly R. Kosiarek https://orcid.org/0000-0002-6115-4359
Elisabeth Newton https://orcid.org/0000-0003-4150-841X
Megan Bedell https://orcid.org/0000-0001-9907-7742
David W. Latham https://orcid.org/0000-0001-9911-7388
Jessie L. Christiansen https://orcid.org/0000-0002-8035-4778
Michael L. Calkins https://orcid.org/0000-0002-2830-5661
Avi Shporer https://orcid.org/0000-0002-1836-3120
Jennifer Burt https://orcid.org/0000-0002-0040-6815

Joseph E. Rodriguez https://orcid.org/0000-0001-8812-0565
Courtney D. Dressing https://orcid.org/0000-0001-8189-0233
John H. Livingston https://orcid.org/0000-0002-4881-3620
Erik A. Petigura https://orcid.org/0000-0003-0967-2893
Jason Dittmann https://orcid.org/0000-0001-7730-2240
David Berardo https://orcid.org/0000-0001-6298-412X
Howard Isaacson https://orcid.org/0000-0002-0531-1073
Andrew W. Howard https://orcid.org/0000-0001-8638-0320

References

Barentsen, G., & Cardoso, J. V. d. M. 2018, Kadenza: Kepler/K2 Raw Cadence Data Reader, Astrophysics Source Code Library, ascl:1803.005
Barnes, S. A. 2007, ApJ, 669, 1167
Buchhave, L. A., Latham, D. W., Johansen, A., et al. 2012, Natur, 486, 375
Cabrera, J., Csizmadia, Sz., Montagnier, G., et al. 2015, A&A, 579, A36
Choi, J., Dotter, A., Conroy, C., et al. 2016, ApJ, 823, 102
Ciardi, D. R., Crossfield, I. J. M., Feinstein, A. D., et al. 2018, AJ, 155, 10
Colless, M., Dalton, G., Maddox, S., et al. 2001, MNRAS, 328, 1039
Crossfield, I. J. M., Ciardi, D. R., Isaacson, H., et al. 2017, AJ, 153, 255
Crossfield, I. J. M., Ciardi, D. R., Petigura, E. A., et al. 2016, ApJS, 226, 7
Crossfield, I. J. M., Petigura, E., Schlieder, J. E., et al. 2015, ApJ, 804, 10
David, T. J., Crossfield, I. J. M., Benneke, B., et al. 2018, AJ, 155, 222
Deleuil, M., Aigrain, S., Moutou, C., et al. 2018, arXiv:1805.07164
Dotter, A. 2016, ApJS, 222, 8
Dressing, C. D., Newton, E. R., Schlieder, J. E., et al. 2017a, ApJ, 836, 167
Dressing, C. D., Vanderburg, A., Schlieder, J. E., et al. 2017b, AJ, 154, 207
Fulton, B. J., Petigura, E. A., Howard, A. W., et al. 2017, AJ, 154, 109
Fűrész, G. 2008, PhD thesis, Univ. Szeged, Hungary
Gaia Collaboration, Brown, A. G. A., Vallenari, A., et al. 2018, A&A, 616, A1
Gaia Collaboration, Prusti, T., de Bruijne, J. H. J., et al. 2016, A&A, 595, A1
Howell, S. B., Sobeck, C., Haas, M., et al. 2014, PASP, 126, 398
Huber, D., Bryson, S. T., Haas, M. R., et al. 2016, ApJS, 224, 2
Kreidberg, L. 2015, PASP, 127, 1161
Mayo, A. W., Vanderburg, A., Latham, D. W., et al. 2018, AJ, 155, 136
Močnik, T., Anderson, D. R., Brown, D. J. A., et al. 2016, PASP, 128, 124403
Montet, B. T., Morton, T. D., Foreman-Mackey, D., et al. 2015, ApJ, 809, 25
Morton, T. D. 2015, isochrones: Stellar model grid package, Astrophysics Source Code Library, ascl:1503.010
Moutou, C., Pont, F., Barge, P., et al. 2005, A&A, 437, 355
Nidever, D. L., Marcy, G. W., Butler, R. P., Fischer, D. A., & Vogt, S. S. 2002, ApJS, 141, 503
Obermeier, C., Henning, T., Schlieder, J. E., et al. 2016, AJ, 152, 223
Osborn, H. P., Santerne, A., Barros, S. C. C., et al. 2017, A&A, 604, A19
Parviainen, H., & Aigrain, S. 2015, MNRAS, 453, 3821
Peterson, M. S., Benneke, B., David, T. J., et al. 2018, AJ, 156, 188
Petigura, E. A. 2015, arXiv:1510.03902
Petigura, E. A., Crossfield, I. J. M., Isaacson, H., et al. 2018, AJ, 155, 21
Pope, B. J. S., Parviainen, H., & Aigrain, S. 2016, MNRAS, 461, 3399
Rappaport, S., Lehmann, H., Kalomeni, B., et al. 2016, MNRAS, 462, 1812
Rebull, L. M., Stauffer, J. R., Bouvier, J., et al. 2016, AJ, 152, 114
Rebull, L. M., Stauffer, J. R., Cody, A. M., et al. 2018, AJ, 155, 196
Ricker, G. R., Winn, J. N., Vanderspek, R., et al. 2014, Proc. SPIE, 9143, 20
Santerne, A., Moutou, C., Tsantaki, M., et al. 2016, A&A, 587, A64
Schlieder, J. E., Crossfield, I. J. M., Petigura, E. A., et al. 2016, ApJ, 818, 87
Seager, S., & Mallén-Ornelas, G. 2003, ApJ, 585, 1038
Sinukoff, E., Howard, A. W., Petigura, E. A., et al. 2016, ApJ, 827, 78
Smith, A. M. S., Gandolfi, D., Barragan, O., et al. 2017, MNRAS, 464, 2708
Sullivan, P. W., Winn, J. N., Berta-Thompson, Z. K., et al. 2015, ApJ, 809, 77
Vanderburg, A., Latham, D. W., Buchhave, L. A., et al. 2016, ApJS, 222, 14
Winn, J. N., Sanchis-Ojeda, R., & Rappaport, S. 2018, arXiv:1803.03303
Yu, L., Crossfield, I. J. M., Schlieder, J. E., et al. 2018, AJ, 156, 22